

A Hybrid Battery Cell Voltage Equalizer Considering Thermal Behavior and Capacity Fade Characteristics

by

Alvin Tuan Thanh Huynh

A thesis submitted to the
School of Graduate and Postdoctoral Studies in partial
fulfillment of the requirements for the degree of

Master of Applied Science in Electrical and Computer Engineering

Faculty of Engineering and Applied Science
Department of Electrical, Computer, and software Engineering
University of Ontario Institute of Technology (Ontario Tech University)
Oshawa, Ontario, Canada

August 2023

© Alvin Huynh, 2023

THESIS EXAMINATION INFORMATION

Submitted by: **Alvin Huynh**

Master of Engineering and Applied Science in Electrical Engineering

A Hybrid Battery Cell Voltage Equalizer Considering Thermal Behavior and Capacity Fade Characteristics

An oral defense of this thesis took place on August 21, 2023 in front of the following examining committee:

Examining Committee:

Chair of Examining Committee	Dr. Masoud Makrehchi
Research Supervisor	Dr. Sheldon Williamson
Examining Committee Member	Dr. Vijay Sood
Examining Committee Member	Dr. Tarlochan Sidhu
Thesis Examiner	Dr. Xianke Lin

The above committee determined that the thesis is acceptable in form and content and that a satisfactory knowledge of the field covered by the thesis was demonstrated by the candidate during an oral examination. A signed copy of the Certificate of Approval is available from the School of Graduate and Postdoctoral Studies.

ABSTRACT

The thesis focuses on developing a robust, high-fidelity lithium-ion battery model adaptive to changes in operating temperature, aiming for accurate estimation of state of health (SOH). The thesis proposes two novel methods for lithium-ion battery SOH tracking and estimation using the developed battery model. Furthermore, the thesis introduces a hybrid battery cell balancing topology designed to achieve optimum balancing speed and enhance battery health by reducing temperature rise and frequent battery cycling during balancing. The proposed hybrid balancing topology combines active balancing for cell-to-pack balancing and passive balancing for excess energy dissipation, depending on the current battery state of charge and voltage of individual cells. The suggested balancing strategy enhances balancing speed, and the control strategy is easy to implement. Lastly, the thesis conducts a detailed comparative analysis of passive, active, and hybrid cell balancing topologies to demonstrate the most suitable balancing strategy for an industry-ready battery management system.

Keywords: Transportation electrification; Battery equalizer; Battery modeling; Battery management system; State of health; Battery temperature; Battery charging; Thermal runaway protection

AUTHOR'S DECLARATION

I hereby declare that this thesis consists of original work of which I have authored. This is a true copy of the thesis, including any required final revisions, as accepted by my examiners.

I authorize the University of Ontario Institute of Technology (Ontario Tech University) to lend this thesis to other institutions or individuals for the purpose of scholarly research. I further authorize the University of Ontario Institute of Technology (Ontario Tech University) to reproduce this thesis by photocopying or by other means, in total or in part, at the request of other institutions or individuals for the purpose of scholarly research. I understand that my thesis will be made electronically available to the public.

A handwritten signature in black ink, appearing to read 'Alvin', with a long, sweeping flourish extending to the right. The signature is positioned above a horizontal line.

Alvin Huynh

STATEMENT OF CONTRIBUTIONS

Conference proceedings

A. Huynh, A. Samanta, C. Chetri, L. Anekal, and S. Williamson, “A Smart, Health-conscious, Dual-stage Hybrid Lithium-ion Battery Cell Voltage Balancing Strategy”, Accepted- IEEE Energy Conversion Congress and Exposition (ECCE), Nashville, Tennessee, 2023.

A. Huynh, A. Samanta, C. Chetri, S. Williamson, “Online determination of lithium-ion battery state of health based on normalized change of state of temperature for e-mobility applications”, IEEE Transportation Electrification Conference & Expo (ITEC), Detroit, Michigan, 2023.

C. Chetri, **A. Huynh**, and S. S. Williamson, "A Comprehensive Review of Active EV Battery Cell Voltage Balancing Systems: Current Issues and Prospective Solutions," 2022 IEEE 1st Industrial Electronics Society Annual On-Line Conference (ONCON), kharagpur, India, 2022, pp. 1-6, doi: 10.1109/ONCON56984.2022.10126563.

A. Samanta, **A. Huynh**, M. Sharma, V. Marcis and S. Williamson, “Supercapacitor and Bidirectional DC-DC Converter-based Active Charge Balancing Scheme for Lithium-ion Batteries”, IEEE Energy Conversion Congress and Exposition (ECCE), Detroit, MI, USA, 2022, pp. 1-7.

A. Samanta, **A. Huynh**, N. Shrestha, and S. Williamson, "Combined data driven and online impedance measurement-based lithium-ion battery state of health estimation for electric vehicle battery management systems," 2023 IEEE Applied Power Electronics Conference and Exposition (APEC), Orlando, FL, USA, 2023, pp. 862-866.

A. Samanta, **A. Huynh**, E. Rutovic and S. Williamson, "Rapid Thermal Modeling and Discharge Characterization for Accurate Lithium-ion Battery Core Temperature Estimation," 48th Annual Conference of the IEEE Industrial Electronics Society, Brussels, Belgium, 2022, pp. 1-6.

Prints

A. Samanta and S. Williamson, Technologies and Applications of Batteries, Smart Charging, and Advanced Battery Management Systems for E-mobility, Publisher: River Publishers (Under Review), Contributions to; Chapter 1 Electrical Energy Storage Systems; Chapter 3 Battery Management Systems; Chapter 4 Cell Balancing Techniques

ACKNOWLEDGEMENTS

Writing this master's thesis has been a journey of both academic growth and personal development, and I would like to take this opportunity to express my gratitude to all those who have supported and guided me along the way. First and foremost, I extend my deepest gratitude to my thesis advisor, Dr. Sheldon Williamson, for his unwavering support, invaluable guidance, and insightful feedback throughout the entire research process. His expertise and dedication have been instrumental in shaping the direction of this work.

I am grateful to my colleagues and friends in the STEER group and Ontario Tech Racing who have been a source of inspiration and encouragement throughout this journey. Their insightful discussions and shared experiences have contributed significantly to the development of my ideas. I would like to express my heartfelt thanks to my family for their unwavering support, understanding, and encouragement. Their belief in my abilities has been a constant motivation, and I am truly grateful for their sacrifices that allowed me to pursue my academic aspirations.

In conclusion, this thesis would not have been possible without the collective support, guidance, and inspiration from various individuals and entities. Each one has played a pivotal role in shaping both my academic and personal journey, and for that, I am sincerely thankful.

TABLE OF CONTENTS

Thesis Examination Information	ii
Abstract	iii
Authors Declaration	iv
Statement of Contributions.....	v
Acknowledgements	vi
Table of Contents	vii
List of Tables	xi
List of Figures.....	xvi
List of Abbreviations and Symbols	xxvi
Chapter 1. Introduction.....	2
1.1 Problem Statement and Motivation.....	4
1.2 Scope of Research	4
1.3 Objectives	5
1.4 Thesis Outline	5
Chapter 2. Literature Review.....	6
2.1 EV Battery Management Systems.....	6
2.1.1 Battery Performance Homogenization Methods.....	8
2.2 Battery Balancers.....	9
2.2.1 Passive Cell Balancing.....	10
2.2.2 Capacitor-Based Cell Balancing	11
2.2.3 Inductor-Based Cell Balancing.....	12
2.2.4 Transformer-Based Cell Balancing	12
2.2.5 DC-DC Converter	13
2.2.6 Power Flow	14
2.2.7 Hybrid Balancing Methods.....	15
2.2.8 Resistive Hybrids.....	15
2.2.9 Dual Active Hybrids.....	16
2.2.10 Supplemented Hybrid Balancers	17
2.3 Battery Characteristics.....	19
2.3.1 Battery Chemistries.....	20
2.3.2 Degradation Factors	21

2.3.3 Battery Equivalent Models	24
2.4 Summary.....	27
Chapter 3. Battery Modeling and State Estimation	28
3.1 Capacity Fade Due to Dynamic Operating Temperature	28
3.2 SOH Estimation Techniques	28
3.3 Battery Impedance to State of Health Prediction	29
3.3.1 EIS Equivalent Model of Lithium-ion	29
3.3.2 Results of Impedance State of Health Estimator	31
3.4 Battery Thermal-SOH Model	34
3.4.1 Battery Thermal Model to State of Health	34
3.4.2 Thermal-SOH Results.....	35
3.5 Summary.....	37
Chapter 4. Hybrid Battery Development	38
4.1 Initial Conditions	38
4.2 Experimental Setup	39
4.4 Passive Balancer.....	40
4.5 Active Balancer	41
4.6 Hybrid Balancer Design	45
4.6.1 Balancer Control.....	46
4.6.2 Continuous Conduction and Discontinuous Conduction Modes.....	47
4.6.3 DC/DC Converter Design.....	47
4.6.5 System Efficiency	50
4.6.6 Simulation Results and Discussion.....	51
4.7 Comparison.....	56
4.8 Summary	57
Chapter 5. Conclusions	58
5.1 Future Work	59
REFERENCES	61
Appendices.....	72
Appendix A.	72
Publications	72
Appendix B.	74

LIST OF TABLES

CHAPTER 2

Table 1 Components and different assembly structure of an EV battery pack.....	6
--	---

CHAPTER 4

Table 2 Nameplate Information of Samsung 40T INR21700 LIB Cell.....	38
Table 3 Starting State of Charges for charge and discharge	39
Table 4 list of active switches during charging and balancing	43
Table 5 List of active switches during Discharging and balancing	43
Table 6 list of active switches during charging and balancing	47
Table 7 Balancer simulation comparison.....	56

LIST OF FIGURES

CHAPTER 1

Figure 1 The adoption rate of electric vehicles for the period of 2016 to 2022.....	2
Figure 2 Basic battery life cycle	3

CHAPTER 2

Figure 3 Hierarchal dataflow and control	7
Figure 4 Basic BMS structure.....	8
Figure 5 Passive equalizer.....	10
Figure 6 Flying capacitor balancer	11
Figure 7 Switched Inductor Cell Balancer	12
Figure 8 Transformer-Based Cell Balancer	13
Figure 9 Buck-Boost balancer.....	13
Figure 10 battery degradation loop	22
Figure 11 Battery normalized capacity face with different ambient temperatures	23
Figure 12 : Basic electrical equivalent model of a Li-ion battery.....	25
Figure 13 Flowchart of the impedance measurement-based battery SOH estimation scheme.....	30

CHAPTER 3

Figure 14 D&V BCT-150 Battery Cell Tester and the EIS data collection Protocol	31
Figure 15 Battery impedance (a) real part (b) imaginary part at a different level of cell SOC and charging cycle.....	32
Figure 16 Cell impedance (a) At different frequency and charging cycle (b) Variation of impedance at 1 Hz.....	32
Figure 17 Capacity fade estimation results	33
Figure 18 Equivalent thermal model of LIB.....	34
Figure 19 thermal model considering battery aging and temperature	35
Figure 20 For 25 degrees Celsius (a) Relation between temperature difference per second and temperature difference with SOH (b) Normalized temperature change for different C rates	35
Figure 21 For 1C SOH and temperature rise at different starting temperatures	36
Figure 22 (a) Internal resistance vs. temperature rise and (b) Time taken to discharge per SOH.....	37

CHAPTER 4

Figure 23 Hardware setup	39
Figure 24 SOC of passive balancing.....	40
Figure 25 Temperature of passive balancing	41

Figure 26 Voltage and current of passive balancing	41
Figure 27 C2P2C with super capacitor balancer.....	42
Figure 28 Balancing performance of the super capacitor balancer during (a) charging SOC, (b) discharging period SOC, c) charging cell temperatures, d) discharge cell temperatures	44
Figure 29 Hybrid C2P and passive cell balancing topology	45
Figure 30 hybrid balancing algorithm.....	46
Figure 31 Flyback converter	48
Figure 32. SOC during charging	51
Figure 33 Battery current during charge	52
Figure 34 Cell temperature during charging	53
Figure 35 Charge DC/DC input (left) and DC/DC output (right).....	53
Figure 36 Charge SOC difference, voltage difference.....	54
Figure 37 Discharge voltage and current	55
Figure 38 Discharge SOC	55
Figure 39 Super capacitor C2P2C balancer	74

LIST OF ABBREVIATIONS AND SYMBOLS

AC	Alternating Current
ACB	Active Cell Balancing
BMS	Battery Management System
C2C	Cell to Cell
C2P	Cell to Pack
C2P2C	Cell to Pack to Cell
CBCB	Capacitor-based cell balancing
CC	Constant Current
CCCV	Constant current Constant Voltage
CV	Constant voltage
DC	Direct Current
DC2C	Direct Cell to Cell
ECM	Equivalent Circuit Model
EIS	Electro Impedance Spectroscopy
EOL	End of Life
ETCM	equivalent thermal circuit model
ETM	Electro Thermal Model
EV	Electric Vehicle
IBCB	Inductor-based cell balancing
LFP	Lithium Iron Phosphate
LIB	Lithium-ion Batteries
NCA	Nickel Cobalt Aluminum
NMC	Nickel Manganese Cobalt
P2C	Pack to Cell
PCB	Passive Cell Balancing
RUL	Remaining Useful Life
SC	Super Capacitor
SOC	State of Charge
SOE	State of Energy
SOH	State of Health
VI	Voltage, Current
VIT	Voltage, Current, Temperature

Chapter 1. Introduction

Lithium-ion batteries are currently the most favored battery type due to their many beneficial properties, such as high specific power and nominal specific energy compared to other electrical storage chemistries or methods. Unfortunately, with this switch to higher battery usage an increase in new material consumption to satiate the demand. As of 2022, there were 18 million electric vehicles, a sharp increase from 2020 where 6.8 million EVs were in usage [1], showing a continuous interest into the future of EVs. For an estimate on the worth of those batteries, assuming vehicles with an approximate of 5000 lithium-ion cells per car, using the popular Tesla 60 kWh pack [2], normally an EV battery will be replaced every 8-10 years or after a loss of 20% to 30% of its original SOC [3]. Approximating a cost of \$4 per cell, in the next 10 years this would have \$23 billion worth of batteries retire from their primary life, excluding depreciation [4].

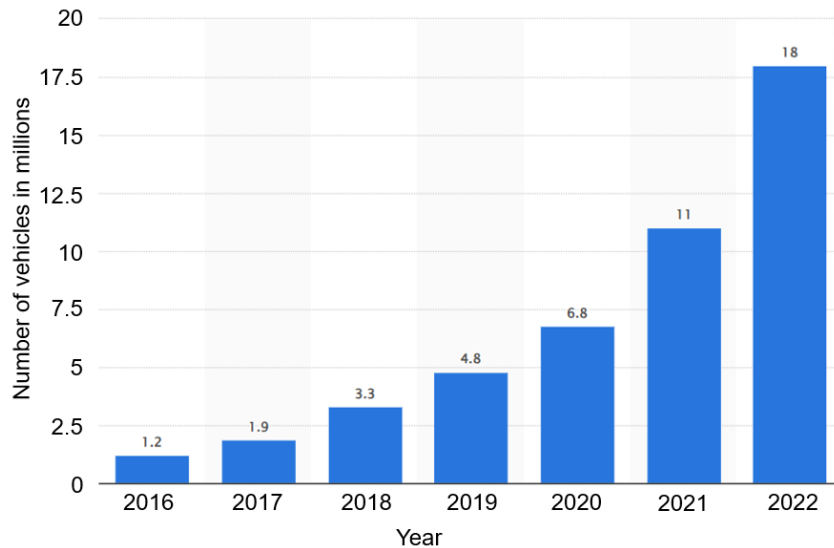


Figure 1 The adoption rate of electric vehicles for the period of 2016 to 2022

This meteoric rise and adoption of EVs will put an extreme strain on metal acquisition and the systems needed to dispose of these cells. Since these vehicles are already in circulation, they will need to be dealt with after their expected usage. The four possible options are direct disposal, reduce of production, reuse/second life implementation, or recycle. With reduction this could be handled in two main methods, either reducing the overall consumption of EVs or reduction of expensive metal usage. As was stated in the consumer EV growth chart, slowing the trend of EV growth is an unlikely scenario as more consumers are looking for alternative energy storage solution usage away from fossil fuels for financial and environmental reasons. For reduction of expensive metals, research is underway for economical battery alternative such as sodium [5] or potassium batteries

[6]. Unfortunately, the preexisting vehicles would already have Li-ion batteries accumulator built and accruing the costs. This leaves three options left to deal with spend batteries: direct disposal, reuse, and recycling. Figure 2 shows the ideal usage life cycle of a lithium-ion cell from extraction of a mine, material processing, primary then secondary life cycle and finally the material would be ideally recycled for more batteries.

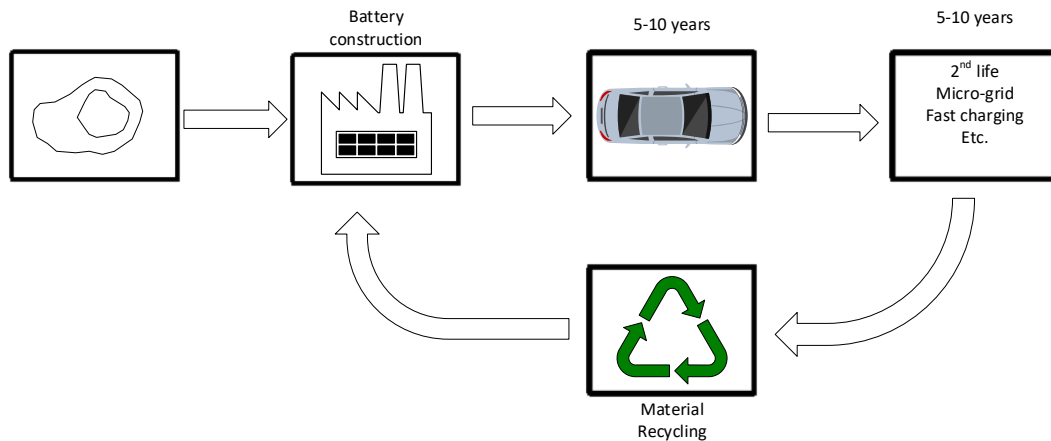


Figure 2 Basic battery life cycle

Currently, only 5% of LIBs are disposed of properly in a recycle facility, thereby meaning that close to 250 000 metric tons of LIBs in 2017 alone are headed for landfills [7], [8]. Reused batteries would only take an even smaller percentage of discarded batteries so assumptively the combination of both recycling and reuse would still only amount to 6% of total batteries discarded from primary EV life.

The major concern in addition other than the material loss of rare earth metals, disposed batteries inherently are dangerous due to their high energy density as well as heavy metals during breakdown and leaching the surrounding areas. The internal electrolyte materials are highly flammable leading to an increased risk of explosion especially in an unmonitored landfill [9]. The long-term effects of incorrect battery disposal are the heavy metals leaching into the ground and surrounding waters leading to decreased environmental quality and harm to human health [8]. For example, lithium salt is very harmful to the lungs, and corrosive to any extremity [10]. Even with correct battery disposal, the methods are generally just large-scale smelting or combustion of the cells. This can produce a lot of toxic gasses such as CO, HCL, SO₂, etc. [11]. Combined with the harmfulness as well as the general aversion to proper waste disposal in developed countries due to safety

standards, this leads to poor countries taking the brunt of disposal which is immeasurably unfair.

An extension of a battery's life is very dependent on primary life usage conditions for second life applications. There are a limited number of active methods to increase a batteries life extension during its primary life cycle, sorting, characteristic clustering, reconditioning, battery balancers, and usage conditions. The clearest and economical method is utilizing a battery management system and equalizer to assist in protecting and managing the batteries properties.

1.1 Problem Statement and Motivation

The effective goal of reuse or reduction of battery consumption is to continue optimizing the utilization of pre-established products for future economic reclamation and environmental considerations. The primary life of an EV vehicle performs within its ideal range of 100%-80% for about 8-10 years with adequate monitoring and maintenance, the secondary life starts from 80% to as low as 40% SOC in limited usage cases [12]. For either primary or secondary life an effective BMS must be implemented, it is the only method to be able to sufficiently coordinate the volume of batteries within an EV to behave similarly and therefore, degrade at a similar rate. That mentioned, cells will still drift in performance from each other regardless of if all cells are utilized equally due to differences in minute usage conditions or within the manufacturing process itself. To reduce performance drift, extensive research has been conducted on degradation reduction and capacity optimization utilizing cell modeling and hardware solutions.

1.2 Scope of Research

The objectives of industrial cell balancers have been primarily speed of balancing, control simplicity, and low financial burden. The scope of this thesis is a battery balancing topology which functions in either charge or discharge mode that allows the cell to maximize usable pack capacity while reducing heat generation of the batteries. The objective of this thesis is to use a combination of active and passive balancing methods to capitalize on the excess energy of higher charged batteries, assist in increasing the rate of charge of the lower charged batteries, reduce heat generation and reduce the time needed to charge in constant voltage (CV) charging period. This will ensure that the lower charged

battery will charge to full at near the same speed preventing premature activation or extended duration of CV mode.

1.3 Objectives

The objectives laid out for this research to investigate:

- To understand the application of batteries to EV, capacity fade effects and protection systems for degradation reduction.
- Develop and analyze an EIS to SOH comparative model.
- Develop a temperature to SOH model for high SOH accuracy considering adaptable to modern needs, high C rate, wide range of operating temperatures, and minimal complexity.
- Develop a battery balancer topology with interest in low temperature rise, fast balancing reduction of control complexity and high balancing accuracy.

1.4 Thesis Outline

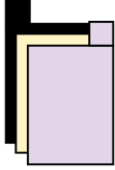
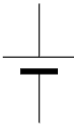
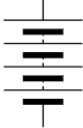

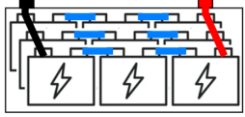

- Chapter 1: Introduction of problem statement
- Chapter 2: Current battery equalizer topologies and methodology will be reviewed and compared for functionality and beneficial aspects.
- Chapter 3: Analysis of battery modeling, chemistry, degradation, and state of health models from literature along with creation, design of state of health models for long term tracking and estimation of a battery. Simulation of the battery model and functionality to BMS will also be included.
- Chapter 4: The hybrid balancing system is developed, simulated, and efficiency will also be analyzed with comparison to previous topologies.
- Chapter 5: Conclude the thesis material, findings, and contributions. Future work will also be listed for proposal.

Chapter 2. Literature Review

2.1 EV Battery Management Systems

To control the complexity of all the internal and external interactions of batteries, the conditions in which they are allowed to operate must be strictly controlled for safety and maximizing performance. This performance aspect can be selected based on the desired need of the system, for instance, stationary battery electric storage systems may prefer reliability and long life while a performance EV may lean towards high control accuracy and instantaneous power. Therefore, BMS need flexible functionality such as a telemetry and control unit responsible for load control, cell level temperature detection, safety limitations and a data logger for cell behavior prediction. Since batteries systems are essential upwards accumulation of electrochemical cells, clear delineation of actual control can be exerted at the different levels shown in Table 1.

Table 1 Components and different assembly structure of an EV battery pack

Mono-cell	Cell /battery	Module	Pack	Accumulator	Application
					
Basic cell chemistry	Parallel stack of mono-cells	series connections of batteries	Series/parallel connections of modules	Series/parallel connections of packs	Application of accumulator to a load or charger
- No direct control	-Internal fusing	- Individual cell fusing - Balancers	- Pack fuses - Balancers	- Full system fuse - Isolation relays -System temperature control	- Sub-system fuses
No readings	- V reading	- Sampled T readings	-Pack VT readings	-System VIT readings	-Load/ charger profiles

Each level will allow a variable amount of direct control impact, with different implementation of adjustment having more discernible impact as show in in Table 1. For example, a single cell with lower may not be greatly noticeable by the pack as other cells will make up the incremental noticeable difference at that level. The general control scheme is likewise broken-down dependent on relative need to limit informational overload or processing requirement on core control units or overwhelm the vehicle driver shown in Figure 3. Specific cell monitoring or estimation is still necessary since a single failed cell can cause total failure and a battery fire.

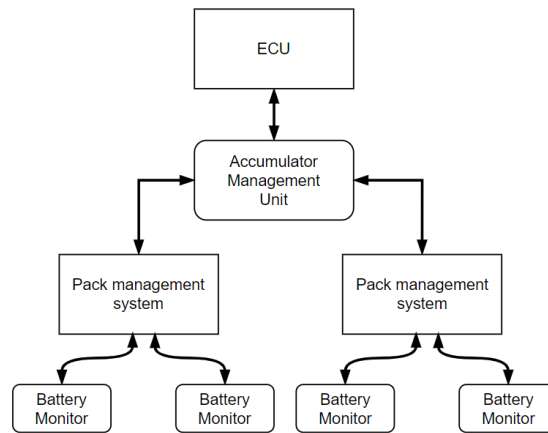


Figure 3 Hierarchal dataflow and control

A simplified BMS is shown in Figure 4 of the core components of a BMS. The typical structure is built upon the battery monitor and microprocessor to allow for the monitoring and processing of the battery string telemetry. Most BMS will have an internal cell equalizer utilizing internal MOSFET based passive balancers such as the AD LTC6804 or TI BQ7961 balance between 8 – 240 mA and up to 400 mA by the BQ25887. Other available option for cell equalization from such as the LT8584 tend to use per cell flyback dc-to-dc converters for multifunctional cell to cell or cell to pack balancing and increase average balancing discharge to 2.5A. Although very the balancing time can be kept low with larger energy transfer, utilizing a transformer per cell is not economical and adding significant weight per each cell.

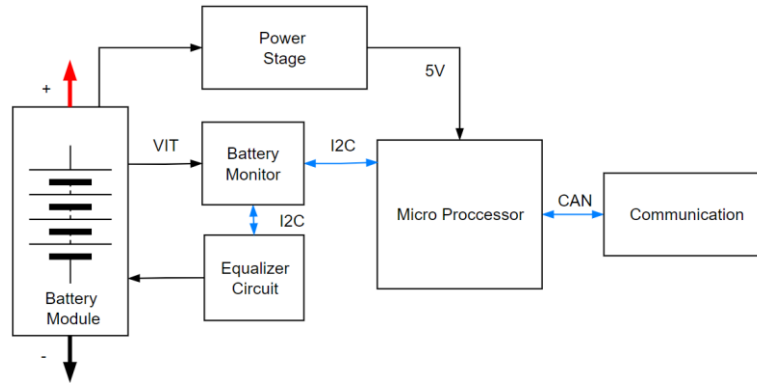


Figure 4 Basic BMS structure

The battery modeling and prediction can possibly be stored on two different levels, either the BMS microprocessor or at a higher tier with the electronics control unit (ECU). With expectations of higher protection, the model should be locally stored per each BMS for faster reaction time. Higher accuracy models may perform but should be relegated to the ECU or online service for higher fidelity. As the models are typically designed for speed, BMS tend to have little tracking or good estimation of a cell's degradation due to higher model complexity or storage requirements.

2.1.1 Battery Performance Homogenization Methods

Outside of active BMS cell performance homogenization, there are some techniques to assist in ensuring the cell have similar characteristics and performance. One method, reconditioning, attempts to reduce internal pack imbalances of the same set of cells. Typically reconditioning is performed in the transition or shift window of primary to secondary life.

The reconditioning method involves cycling the pack over long durations to slowly converge all cells internal resistance and performance for higher predictability. The cycles will subject the higher performing cells to greater load to degrade the cells to match worst cells. The advantage of this method is ease of implementation as no alternation to the packaging of packs is needed, the only adjustment would be implementing to the control algorithm for the reconditioning algorithm. The method claims to reducing imbalances of about 4% internal resistance difference in about 1 months for a shift from the initial life to the accumulator second life [13]. A clear downfall of the system is that it still retains the worst aged cells within the pack Overall, the method reduces the best cells to account for

the performance difference in the worst cells, this giving an overall pack life of 15 years which may still be better than the original of 8-10 years [14].

In the second method, by mapping cells based on their expected or nominal values they can then be grouped or clustered with other cells of similar [15], [16]. This typically has the benefit of rooting out bad cells before conversion into a second life and therefore would increase the packs lifespan by reducing the lower RUL limit. Sorting/clustering functions by setting an initial target point into each supposed cluster of similar cells then checking the variance of each cell from the center point. At this point it runs a check to validate if the center has a low deviation and if other cells may fall into cluster groups. In each iteration it approaches what it believes to satisfy the minimum number of similar characteristics then group the cells per each central node. The drawback of this system is the need to take apart the whole accumulator to be able regroup the cells. This will incur additional cost in terms of sorting and a further loss of product as some cells will be further discarded due to low expected future performance or visible deformation. It still produces a better product as the cell will not be overly cycled between each life application and more likely to have a longer future operation time then reconditioning.

Both methods are typically performed in transitional periods of the cell's life, either during original assembly of a battery pack or in the shift to second life. The best method would be to manage the direct utilization of the cells during its primary life. The only clear option would be to utilize power electronics to manipulate the cell loads and performance characteristics.

2.2 Battery Balancers

For hardware implementation the most important auxiliary safety and performance tuning circuit is the battery equalizer. It functions as the actuation of maintaining preferable or similar battery performance between cells in terms of voltage, state of charge (SOC) or more recently state of energy (SOE). The secondary function is to assist in increasing the usable capacity of a battery by reducing the pre-mature activation of safety features such as over-voltage from the highest charged cell during charging or under voltage from the least charge cell in discharge mode. If not properly managed the unbalanced cells reduce the effective capacity of the battery pack, hence an effective cell balancing scheme is

essential. Balancers are particularly useful for regenerative braking, where the charging and discharge periods are minute and the voltage limits are more vulnerable during motoring mode [17]. Equalizer fall into two main categories: passive and active balancing.

2.2.1 Passive Cell Balancing

Passive cell balancers (PCB) utilize bleed resistors to burn off excess energy when comparing the capacities of the rest of the pack. In this method only the lowest charged cell is protected. If there are any voltage or SOC variations, all other cells will undergo balancing and burn off excess potential. The equalizer is completely inefficient as it does not recover any charge and releases the energy as heat which then requires the balancer to have a heat management system. This heat also adds to the overall temperature of the battery system, which is not ideal for continual usage. Also, since the only component is a resistor, it does not innately come with its own filter, which may result in some higher ripples compared to the other equalizers. Resistive cell balancing techniques are of the following types, fixed shunt resistor cell balancing and switched shunt resistor cell. In many cases the control loop designed is extremely simple; a passive balancer typically only observes that there is a charge difference, or the voltage limits and then commences balancing. In many cases the control loop designed is extremely simple, a passive balancer typically only observes that there is a charge difference in addition to the voltage limits, and then commences balancing.

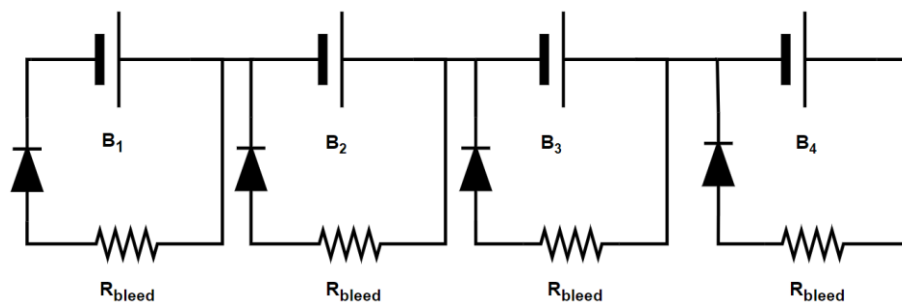


Figure 5 Passive equalizer

2.2.2 Active Cell Balancing

Unlike PCB, active cell balancing (ACB) uses a charge transfer method from one cell to another to retain a similar charge in all the connected cells by using capacitors, inductors, transformers or converters [18], [19]. Unlike PCB, active balancing of cells reduces energy

from being dissipated thermally and can either reduce the charging time or increase the capacity during discharge [20], [21]. As a result, their speed of operation and efficiency has increased, but at the same time making them highly complex and expensive. ACB can be categorized into capacitor-based, inductor-based, and convertor-based.

2.2.2 Capacitor-Based Cell Balancing

Capacitor-based cell balancing (CBCB) uses capacitors to balance the charge between the cells. These are of the following types, namely single capacitor, switched capacitor and double-tiered switched capacitor [18], [22]. As shown in Figure 6, in single CBCB also known as a flying capacitor, a single capacitor is used to store excess energy from a higher charged cell and transfer energy to a lower charged cell. The main criteria, namely capacitor capacity and switching frequency are considered when designing them as a smaller capacity capacitor can be used if the frequency is higher. In switched CBCB, the charge from a higher cell gets transferred to the adjacent cell, and the energy gets transferred to the next adjacent cell, gradually balancing all the cells present in the entire pack. In double-tiered switched CBCB, a parallel layer of capacitor is added to the switched CBCB. Here the charge transfer is possible between various cells, making it possible to skip one cell in between two cells. This makes its operation much faster than single and switched CBCB [23].

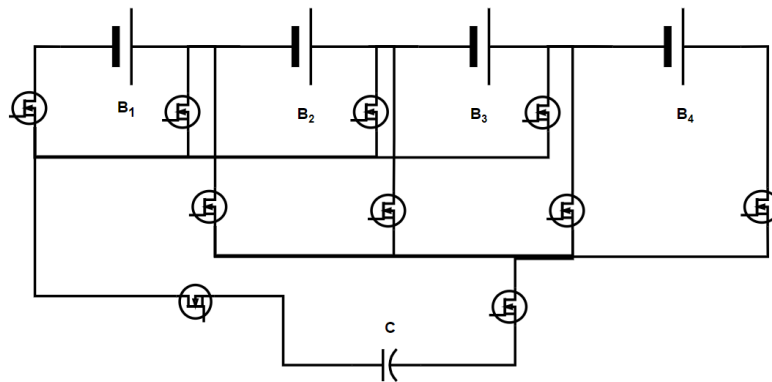


Figure 6 Flying capacitor balancer

2.2.3 Inductor-Based Cell Balancing

In purely inductor-based cell balancing techniques, the categories are listed similarly to capacitor-based balancing such as single inductor or switched multi-inductor balancers. The primary benefits of utilizing inductor balancing over capacitive is higher balancing speed using the same methodology of transferring from high SOC cells to low SOC cells [24], [25]. The topology also has greater control over output voltage due to the variable control over the switches. The disadvantage of this method is the high setup cost compared to capacitor balancing, higher control complexity and poor over-voltage protection near end of charge [26]. A typical diagram of switched inductor cell balancing is depicted in Figure 7. In switched IBCB, the transfer of charge is possible between neighboring cells, gradually balancing all the cells present in the pack [27]. The disadvantage of this method is that the time taken for balancing is directly proportional to the number of batteries in the overall chain as energy may need to travel between all cell if the highest and lowest are furthest part.

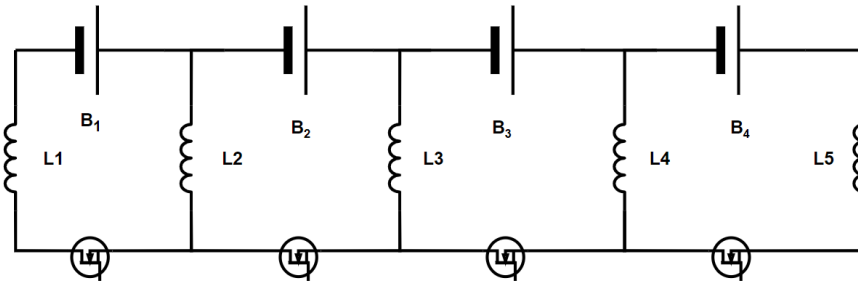


Figure 7 Switched Inductor Cell Balancer

2.2.4 Transformer-Based Cell Balancing

Another industrially preferred option is transformer-based equalizers, which utilize either single cell transformers or specialized multi winding transformers [28], [29]. The operation with flyback transformer will take excess energy to either redistribute throughout the entire pack or utilize a shared bus line to directly connect to the lowest charged cell. The system has many benefits such as isolation, simpler control, ease of implementation, ripple protection, and market availability. The drawbacks such as increased cost, weight and low scalability make it an uneconomical option [30]. A typical diagram of transformer-based cell balancing is shown in figure 8.

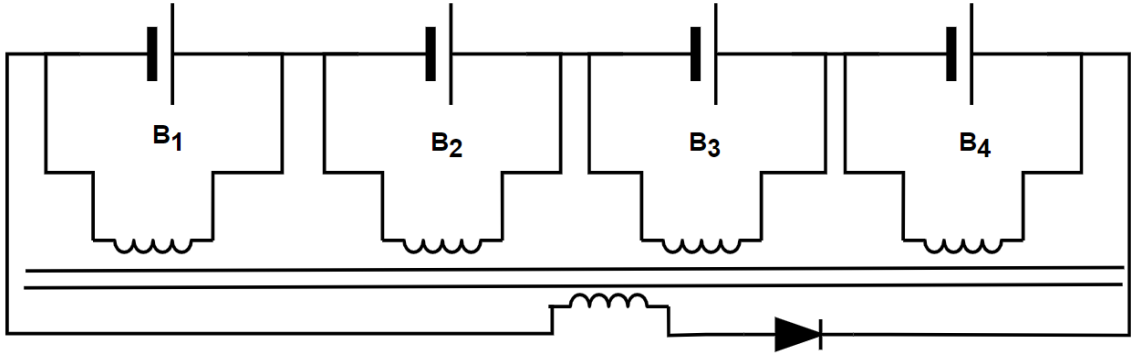


Figure 8 Transformer-Based Cell Balancer

2.2.5 DC-DC Converter

Stepping into DC/DC converter-based equalizers, these topologies utilize non-isolated converters to transfer energy from adjacent or neighboring cells [31]. Since the operation is only between neighbors the balancing can be performed relatively quickly, the caveat is if the most charge imbalance is between the cells further on the string the energy must pass through each converter. With the inclusion of both capacitors and inductors, the topology can mitigate the effect of inrush current as well as reduce the chance for over voltages. Other benefits such high efficiency, higher accuracy, large voltage differences, bidirectionality and low ripple make it very suitable for fast balancing. All of this is traded for higher component cost, increased control system complexity, increased duty cycle and more processing power requirement [32], [33].

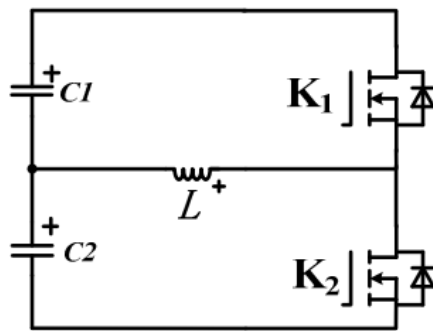


Figure 9 Buck-boost balancer

One example is Buck-Boost balancer which used the principle of non-isolated buck boost converter to balance the cells. The operation of this topology can use the same operating conditions as a regular buck-boost [34]. Buck-boost balancers have the option not to use

filtering capacitors for adjacent cell balancers since the cells can substitute the behavior. This topology can then utilize only inductors and MOSFETs assisting to reduce cost and system complexity. There are more variations of DC/DC balancers but those are less preferred due to a complex control methods, greater number of inductors used and lack of voltage ripple protection without the filter [35].

2.2.6 Power Flow

Another way to analyze equalizer topologies is based on the method of energy transfer or power flow. Active cell balancing topologies can be categorized as Adjacent Cell to Cell (AC2C), Directed Cell to Cell (DC2C), Cell to Pack (C2P), Pack to Cell (P2C), Multi Cell to Multi Cell (MC2MC). In adjacent-cell-to-cell based equalization methods, the excess energy is shuttled to and from adjacent cells, which lowers control complexity since the comparisons are between adjacent cells [36]. The main drawback, is if the targeted low cell is positioned further away, the energy would still need to travel through all the neighbors cells before reaching the low cell greatly increasing balancing time and lowering efficiency [37]. DC2C utilizes a direct power transfer link from a higher charged cell right to the lower charged cell [38]–[40]. Capacitor-based topologies and traditional single inductor-based topologies are mainly used in AC2C and DC2C cell balancing [41]. In C2P balancing method, the excess energy of the highest charged cell is redistributed to battery pack or even smaller select battery strings[42], [43]. Other benefits of C2P include utilization in both charge and discharge cycles, in charge it assists with throttling charge rates of higher cells and in discharge it utilizes the excess energy to independently take on some of the pack draw. C2P is still more typically used in charging since the efficiency to boost a small amount from one cell to the pack is not that high [44]–[47]. One of the drawbacks of C2P is redistribution of energy back into the highest SOC cell causing a point of inefficiency.

Inversely, in P2C balancing, energy is taken from the entire battery pack and transfer the energy to the most-depleted cell in that string. The same type of draw back is present where information of individual cell voltage, SOC are typically required along with a complicated control logic. P2C balancing methods are more efficient when assisting lower charged cells during discharging by connecting the energy shuttle in parallel with the lowest SOC cell, and load sharing with the battery. However frequent charging and discharging of battery

pack imposes detrimental effect on battery life and pulling energy from the pack also includes the targeted cell. MC2MC equalization methods [48] function similar to DC2C, but is upscaled for battery strings. This is more efficient with larger packs where this is possible, the drawback of this system requires more accurate cell monitoring and more complex controls to accommodate large energy transfers.

2.2.7 Hybrid Balancing Methods

Since balancing methods have regions, they are more efficient in function, newer topologies will tend to include more than one topology or power flow to maximize balancing during charge or discharge. Purely single method active balancers function more efficiently with packs of medium or large variation where the full transfer of each cycle can be appreciated. As such at lower pack variation or nearing the end of their targeted zone, active balancers tend to over correct and therefore become far more inefficient. The methods to correct this will over complicate the system increasing cost and complexity if the topology at this point has not become a hybrid solution anyways. Here the hybrid active and passive balancer can utilize the full range of SOC. Given the CCCV charging method, the active topology balances the cells efficiently in CC mode with larger voltage variations, while the passive topology balances the cells at lower voltage variations at end of CC to CV mode.

2.2.8 Resistive Hybrids

Due to the low cost and adequate performance, resistive balancers will typically be the main implementation for a topology or power flow-based hybrid balancer. Since the complexity is low and passive balancers can be implemented per battery, it can be slotted in all topologies. The topology also provides robustness that may assist other topologies that have issues with small variation or systems with inadequate protection of over voltage or inrush current balancing issues such as primarily single component systems.

The low rate of equalization by passive systems makes them only reasonably functional for small battery variations and during CV mode. The best utilization for resistive equalizers would be for finite balancing of the system near end of charge when the charge current is already low and SOC variation should be at a minimum. This would dictate general zones of operation between the active and passive balancer during charging, where the active

equalizer would balance larger variations during CC or other high current modes and passive balancing would further reduce variation during CV and slower periods. Such a system would be marginally slower than a fully active balancer but would be able to balance to a higher tolerance as well as balance during idle operation where other systems would still have a large loss.

Another method of utilizing passive balancers in a hybrid system would be concurrent usage of the active and passive balancer. The bypass ability of the balancer could reduce the charging rate of non-targeted or higher SOC cells, while the lowest SOC cell would then be charged with assistance from the active balancer. The drawback of this system would be the increase in overall charge time, power losses through heat and higher complexity of active control. The benefits would be a nominally faster balancing time, which may also speed up overall charge time by reducing fine balancing in CV mode.

2.2.9 Dual Active Hybrids

Dual active hybrid system comprises methods that utilize two or more pre-existing topologies/concepts and merge them into one equalizer. The definition for combining the purely single energy storage-based systems such as utilizing the combined properties of inductors and capacitors for energy shuttling would fall under the power electronics equalizers. Hybrid active equalizers can be more readily compartmentalized by the usage of power flow classification of functions. The distinction also assists with control characterization and system comprehension. For example, a system utilizing adjacent cell to adjacent cell could be paired with a pack to cell topology. Both sub topologies would have overlapped functionality, but each could be specified for a specific goal such as C2C with ensuring the neighbor cells are equal compared to P2C ensuring the maximum variation between cells is low.

The major concern with hybrid systems is the increase in part count and complexity. Many of the topologies may not have overlapping parts, or if they do, it will greatly increase complexity and reduce robustness. Systems such as C2C, P2C or transformer based MC2MC share very little in common and even if combining them increases balancing or charging speed, the control and hardware would be far too complex and prohibitively expensive for realistic implementation. Therefore, matching systems with shared or

complementary features or components would be ideal. For example, pairing C2C with resistive balancing would share the concept of individual based balancing and could switch between either system dependent on the needs. Another clearer example would be P2C and C2P balancing which can share all components with only some additional components. P2C & P2C are also complementary in which cell the topology is targeting and are essentially inverse mechanisms of each other, which assists in reducing function overlap.

2.2.10 Supplemented Hybrid Balancers

Hybrid balancers with an addition of components or concepts external to the contemporary equalizer designs typically use auxiliary topologies in assisting with energy shuttling or other more novel concepts. This could be as simple as utilizing an external battery chemistry or a super-capacitor, which is typically the easiest to implement of the novel designs as historic designs are more easily adapted to external components. Such as utilizing as lead-acid battery in addition to a P2C2P pack balancer [49].

Previously, Friansa et al. [50] proposed a DC-DC boost converter and an auxiliary battery capacitor-based cell balancing scheme where the battery capacitor was used for energy buffer and the DC-DC converter was used to boost the voltage while transferring energy to the lowest cell. The primary drawback of the scheme is the use of additional auxiliary units and the necessity of enough charge before initializing the balancing operation. Sani et al. [51] used two battery cells at the time to charge the buffer capacitor to minimize the low voltage different problem of typical switched capacitor-based schemes. Increased voltage difference for transferring the charge between battery cell to capacitor enhanced the balancing speed. However, one of the primary drawbacks of the scheme is if one cell of the pair has a lower SOC than the average SOC of the pack, then instead of balancing the scheme further discharges the cell instead of charging, resulting more imbalance. In addition, the balancing scheme requires significantly higher number (6x number of series connected cell) of power switches which lead to increased switching losses, bulkiness, and excessive costs. Further, Baronti et al. [52] proposed a supercapacitor and DC-DC converter-based DC2C balancing scheme. The proposed balancing scheme used PMOSFETs that increased the balancing time. Further, the proposed control scheme is overly complex and outdated. Jiang et al. [53] demonstrated a single supercapacitor and cell

bypassing-based balancing scheme where the regenerative braking energy was used to charge the supercapacitor rather than taking the balancing energy from the battery itself to enhance balancing efficiency. One of the primary downsides of the scheme is the online bypassing of the battery cell. This is because typically the discharge current of LIB cells is extremely high. The discharge current could be even higher than 20 C especially in the case of high-power applications. Thus, online bypassing of cells requires costly switches and protective circuits even though it is extremely risky and challenging. Moreover, balancing efficiency and speed is very low as the balancing operation can only be possible during the regenerative braking period.

The current industry favors low cost and complexity and therefore would prefer passive balancing. The speed is extremely low and for larger packs would be entirely unacceptable as a protection and optimization circuit. This results in the overall categories in very polarizing placements with either maximum or minimum scores. Robustness is low since it does not greatly adapt to any situation but can be used to moderately protect from voltage and current ripples from the battery, load, or charger. The topology with the most nominal performance between all the different categories was active balancing. Since the category is very flexible in terms of utilization, it can fit most requirements to a fair degree with specialty in speed. With the industry shifting to smarter BMS and faster charging becoming more commercially available, active balancing stands to be the optimal solution for performance. The drawbacks are typically the higher control complexity to passive and active topologies tend to need higher complexity to function as protection from spikes and ripples.

Hybrid balancing suffers due essentially containing both systems as a single topology. This results in high costs, more parts, and a more complex control scheme. The speed is slightly lower than that of active balancing but the trade off is extremely high balancing accuracy which would be able to reduce variation to below 1%. The drawback of this could potentially be useless to actual industry and implementation as batteries will always drift from each other. Since the complexity of the system is higher than either other option, robustness is very high since it could work as full protection from system spikes and ripples. For performance in this comparison, as a technical model the hybrid topology was

the best for high accuracy, speed, and robustness. For a general statement all the topologies are needed for battery optimization and safety, utilization and specific application will dictate the desired topology.

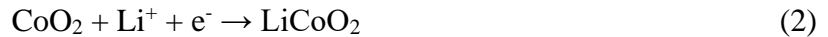
2.3 Battery Characteristics

Electro-chemical cell have had a long and storied history as generations have always stived to store energy, dating back all the way to 1000 BCE with the Bagdad cells [54]. The main components can be broken into three categories: anode, electrolyte, and cathode. The basic function is ionizing particles from the anode, electrolyte acting as a transfer medium for intercalation and deposition of the ionized atom to the cathode. This oxidation reaction will in turn release free electrons from the anode to the cathode generating a usable current. The reversable process or reduction which accepts the election and ion to form an oxide.

Oxidation half reaction, release of electrons and ionization:



Reduction half reaction, reduction, and synthesis of metal oxide:



Full reaction redox:



Within batteries, a separator/permeable membrane material will also be utilized to keep the electrodes apart. This enables batteries to be portable as well as assist reduce the overall size of the battery. Another extra feature of separators can be a inbuilt safety functionality such as restriction of the micropores to reduce the chemical reaction in the event of high temperatures [55]. To note, the selection of a cathode and anode material depends on the nobility of the material. The higher the nobility, the more stable the material is and more suitable as a cathode and the inverse for anodes which are more reactive. Typically, the further away the materials are on the scale the more corrosive the redox reaction is and therefore the more current can be generated just from the two materials.

2.3.1 Battery Chemistries

The general industry currently favors lithium-ion-based cells due to the beneficial properties of a high specific capacity of 3860 mAh/g, low weight, long life, and fast charging compared to its predecessors/competitors of Nickel metal hydride (NimH) or lead acid batteries. There is a differentiation of classification with lithium-metal (LMB) and lithium-ion batteries (LIB), where lithium-metal utilize primarily lithium plate as anode plates such as Li(TM)O_x . Conventional LMBs have fallen out of favor for a long time to many issues such as high growth of Lithium dendrites and low coulombic efficiency [56]. Lithium-ion batteries in contrast utilize graphite to intercalate Li-ions between the graphite layers as well as a Li-ion salt electrolyte allowing the movement of Li-ions reducing the plating on the surface of the anode. Another factor to assist with dendrite reduction is development of a small film of solid electrolyte interface growth (SEI), which is an ionically conductive and electronically insulating solid electrolyte layer on top the anode [57]. The overall performance of Li-ion is still very high with a specific energy around 200 Wh/kg and specific power around 300 W/kg, but this is highly dependent on the specific Li-ion chemistry. such as Lithium Iron Phosphate (LFP), (NMA), LTO, and NMC. Within the current battery market, the range of lithium-ion batteries is expensive since different materials will push the performance to either higher safety, cost reduction, higher specific capacity, or specific power. The other more minor variation is the difference in specific the percentage such as NMC 111 (Nickel 33.3% – Manganese 33.3% – Cobalt 33.3%) compared to NMC 622 (Nickel 60% – Manganese 20% – Cobalt 20%) which trades overall stability for higher performance [58].

A common Li-ion chemistry is lithium Iron phosphate (LPF). Although not an old composition the chemistry has been fairly explored with variations to the innate beneficial properties it has as a lithium cell, at 170 mAh/g and 110 Wh/kg it has a moderate current density, but in return is a relatively low cost, low toxicity and higher safety makes for a suitable battery type for EV usage. The overall chemistry has also been widely experimented with varying effects to increase battery life, thermal resistance or other beneficial property all due to stable chemistry [59]. Analyzing a stressed cell we can also see general properties of lithium cells, at higher temperature or deeper discharge the cell degrades faster resulting in a lower amount of cycles or a worse overall SOH [59].

Optimally the cell should be operated at 25°C with no more than 20% discharge to maximize battery life, but with general populace use this is unlikely. At moderate usage of 40% and above higher temperature an estimated 18000 cycles could be expected of a system. Another note is that the depth of discharge and the formation of internal resistance is not a fully linear relationship but can be model and considered when forming a battery model [60].

2.3.2 Degradation Factors

As degradation is generally the loss in quality and usability of a battery over time, in decision making purposes it is the central characteristic of batteries in determining if it should even be considered for reuse other than cost. Degradation encompasses many internal characteristics such as surface electrolyte growth, capacity fade, calendar ageing, material deposits, mechanical changes, etc. Irrespective of battery chemistry, another form of cell performance drop is from the chemical material process of a battery. For the proper functionality of a battery to work, a small layer of stabilized electrolyte will grow on the surface of the electrode in contact with the electrolyte material. This may not happen immediately after assembly of the cell, so all cells usually need some amount of cycling to activate the internal processes and includes the SEI growth. The mechanism of degradation utilizes electrode materials such as silicone and the electrolyte material, lithium-ion, and will form an alloy such as Li_{15}S_4 along the border of both materials meeting each other. This new alloy will then assist with preventing electrolyte breakdown since the negative electrode material operate outside the window of electro-chemical stability of the electrolyte.

Considering the new alloy is formed within the battery greater than the original substances, a volume expansion will occur, of up to 300% for Li_{15}S_4 [61]. With ageing the limited supply of active material is slowly converted to inert materials that only degrade the performance of the battery since the method of activation and usage are the same process as its degradation. Pores, cracks, air gaps, and crystallization all develop within the cell adding to the internal resistance of the battery as the material dries and changes into a non-uniform surface. Since it does not stop the alloy volume expansion, solid electrolyte interface (SEI) will continuously grow within a battery until total failure or until deemed unfit for further

usage. Of course, all of this can be adjusted or changed depending on factors such as material makeup, particle size, processing care. Representing all the factors mathematically for determining accurate SOH is highly challenging. Thus, more practical phenomena such as rate of temperature rise has been considered in this paper for SOH estimation. Translating degradation into something more familiar and usable for battery system implementation, the loss of active material and therefore available percentage of the usable battery capacity can be called capacity fade. The method of calculating capacity fade is to experimentally measure the reduction of the potential usable charge and discharge cycle of the battery.

The overall degradation can be shown as a cycle of self-degradation with four distinct steps. Starting with an increase to internal resistance by either SEI growth or crystallization would be considered an increase inefficiency. This inefficiency can be simplified to lumped power loss as heat adding to the operational temperature of core material of the cell. This would contribute to increasing the rate of the chemical degradation reaction of the cell decreasing the overall capacity of the battery and closing the loop as positive feedback [62]. The core heat generation can then be transferred through the electrolyte and electrode material to the surface of the battery and then can be accurately measured with physical temperature sensor with relation to the cells surface temperature. Typical degradation loop of LIB is shown in Figure 10. The cycle of battery degradation is a positive feedback loop where the battery's temperature will lead to an increase in internal decay/resistances and a decreased overall battery life. This accelerates each iteration of the degradation process.

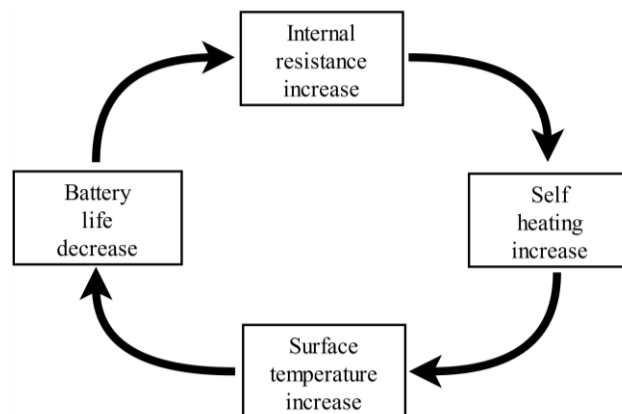


Figure 10 battery degradation loop

Another key aspect for consideration of battery balancers is state of health (SOH), which is a qualitative measure of the capacity fade or degradation. The utility of the parameter assists with monitoring the long-term health or future usability of a battery pack. For the primary life cycle, it assists in ranging the approximate maximum charge of the battery by utilizing internal resistance growth and surface self heating as the measurable parameters [63]. One method to feed temperature data into SOH control system is an implementation of a temperature estimator. In addition to the electro-chemical model, an electro-thermal model would create a more detailed behavior of a lithium-ion battery reducing the need for excess physical sensor which may read incorrectly due to external factors. One implementation of this is combining the typical thermal model for lithium cells with Kalman filters which results in a battery core temperature estimator with high accuracy and easy to implement system. This implementation would suggest for every 0.25°C increase, 5% of the battery is affected leading to some capacity fade [64].

Another unavoidable degrading factor of a battery is calendar life, defined as the capacity loss in storage with low to no active usage. This aspect is uniquely hard to account for or event measure as it revolves around the storage and long-term age of a battery, resulting in the data collection either an extremely long term study, possibly 15 years, or utilizing accelerated ageing techniques.

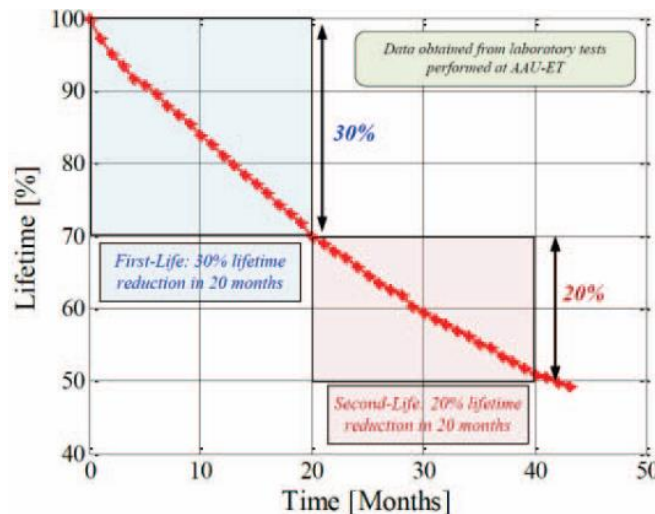


Figure 11 Battery normalized capacity fade with different depths of discharge [65]

Calendar ageing is not the lead degradation in a battery but become more apparent on aged batteries, such as batteries of low-quality batteries or in bad storage conditions. For example, cells stored in high temperatures will have a faster self-discharge. Swierczynski et. al were able to make forward fitting equations for estimating the capacity fade and power fade of a LFP with relatively low error [65].

$$F_{capacity} = K * Time * 0.8 \quad (4)$$

$$P_{fade} = k * t \quad (5)$$

The first equation is for capacity fade where K is dependent on temperature and battery state of charge (SOC). The second is the fitting equation for power fade over time. Both fitting equations are simple to use as the main changing parameters are the k value factoring in temperature and storage SOC. This gives a very fast and low resource intensive model to measure batteries and determine future economic viability of the cell.

2.3.3 Battery Equivalent Models

In EV applications, tracking the performance of all cells is key to be able to accurate balance and protect the cells, the model also need high computational speed. The electrochemical model is the most simplified/adapted to a more suitable purely electrical model, typically a Thevenin open circuit model. This basic model takes the behavioral aspect of the batteries at the terminal and summarizes the interior chemical conditions into more easily understood representative resistances and capacitances as shown in Figure 12. R_0 is the internal resistance of the battery representing solid electrolyte growth, which is consistent over shorter durations over time, but will change depending on the current life cycle. The parallel components R_1/C_1 and R_2/C_2 represent transient parameters such as the internal polarization and diffusion of the cell. More pairs can be added for increased accuracy, but the drawback is slower computation and higher processor requirements. Apart from this model, there are a multitude of variants and method combinations to summarize the electro-chemical model to an electrical equivalency model ranging from the basic Thevenin, impedance, to combinational models each with their own variants depending on the groups usage with error rate between 5-20% [19].

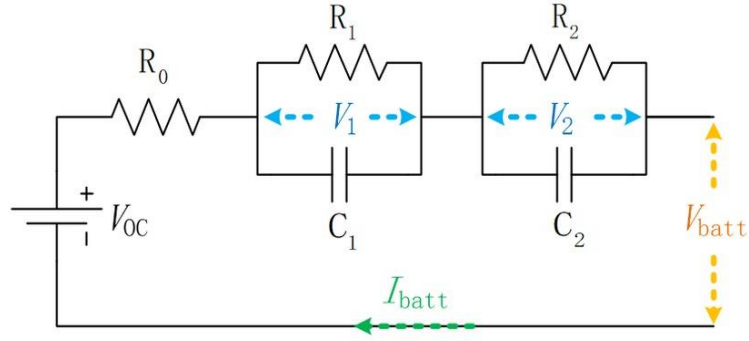


Figure 12 : Basic electrical equivalent model

State of charge (SOC) is keeping track of the current available capacity of the battery compared to the datasheet rated capacity. This is performed by tracking remaining charge of the battery though direct or indirect means. The benefit of keeping track of the charge is more accurate measure of the cycle usability of the battery. The few direct measurements of a battery are current, temperature, impedance (to an extent) and voltage. Unfortunately, since the voltage can be instantaneously affected by many external conditions such as load spikes, temperature and its own internal discharge curve, voltage is a non-linear form of usability tracking. SOC is greatly used by the public to the extent that even those with little to no knowledge of electronics will still refer to their phone usability with percentages or fractions of charge.

$$SOC = \frac{C_{current}}{C_{maximum}} * 100 \quad (6)$$

2.3.4 Coulomb Counting

The most utilized SOC estimation technique is coulomb counting, whereby measuring the current entering or leaving the cell and with tracking the remaining charge changes, the SOC is estimated by subtracting or adding the change from the cumulative net charge. Its generally an effective estimation technique since the premise is simple and results in good accuracy and lower processing power compared to more ECU intensive methods. The drawback of coulomb count are initial SOC input error and continued measurement reading errors. If the starting SOC is incorrect, then the continued estimation will be mis-estimated.

$$SOC(t) = SOC(t_0) + \frac{1}{Q_{rated}} \int_0^t i dt * 100 \quad (7)$$

In coulomb counting the key parameters are the starting SOC(t_0) and the continuous tracking of the of the charge by measuring the current coming n and out of the battery. The clear issue with coulomb counting is lack of adaptability or robustness such as if the initial SOC data point is incorrect if the current information is not smooth or is momentarily cut off and lastly the system does not adapt to cell ageing. All the drawbacks will make Coulomb counting inaccurate and may give misleading information.

2.3.6 Adaptive Approach

At the core of many of these estimators is a Kalman filter, which in effect recursively attempts to filter out any noise from measurement or processing by using a series of relations between linear quadratic equations for estimation [66]. The usage of Kalman filters is quite high due to the ease of use while also working well with basic electrical models and non-linearity of state of charge. The drawback of Kalman filters need large number of computational resources or low KF have relatively low computational efficiency. This holds this method from real time or mass scalability needed for the amount of batteries in an EV, however a lot of research has been dedicated to increasing efficiency and SOC applications [67], [68].

2.3.7 Data Driven

The last major category of estimation methods would be machine learning or data driven methods. This type compiles large amount of collected data from previous experiments to develop an algorithm that correlates the different characteristics into trends and actively readjusts the prediction based on new given data. This system has the benefit to contain a large amount of data from different battery types to develop a universal functional model, but in doing so may need significant storage as well as processing power to effectively run. This method can be simplified if the data and processing is quantized, if the data is calculated prior to implementation into the BMS, or excess data is removed once the neural network has been developed [69].

2.4 Summary

To ensure maximum battery longevity, many considerations must be made to develop an adequate BMS. Understanding a battery model is imperative to accurate battery performance assessment, high accuracy typically means utilizing large databases to either develop complicated machine learning algorithms or increase the complexity of basic Thevenin models. For real time adjustments and estimations, simplicity and quick calculations are typical of the immediate requirement so a 2RC Thevenin model is sufficient and further diagnosis can be performed during low importance time frames. Battery balancers are a primary method for ongoing maintenance of the cells and ensuring long term predictive performance of the batteries. Resistive battery balancers have been the industrial standard for adjusting batteries due to low costs, but the performance, balancing time and absolute power loss is not adequate for modern battery and charging systems. Active balancers are much faster but become significantly more complicated in control and incur high costs to be able to account for all protections as well as fast balancing. Hybrid balancers take from to reduce control complexity but maintain the reliability from passive balancers.

Chapter 3. Battery Modeling and State Estimation

3.1 Capacity Fade Due to Dynamic Operating Temperature

As the SOC reduces, this is called capacity fade and makes the cell discharge quicker without the same relative power as well as decrease the usage of battery. This can be caused by solid-electrolyte interface (SEI) growth and active material loss for both electrodes [13]. SEI is the stabilization reaction of the electrolyte and anode materials which becomes permanently stable resulting in small a small film. This film is unable to contribute to providing potential chemical differences but instead is a lithium alloy which would contribute to the internal resistance. Temperature leads a large part in this process, as it would accelerate the aging of the battery and result in more SEI growth. For instance, at nominal operating temperature at 20°C will have 2300 cycles, when increased to an operating temperature of 50°C the cycle life drops down to 1000 cycles and lastly at 60°C the cell only has 500 cycles, showing an linear relation between temperature and capacity, by approximately losing 44 cycles per 1°C increase [70].

To help preserve the batteries, an ongoing qualitative measurement of a battery's capacity compared to the datasheet helps determine the battery's life cycles as well as how it may perform at any given time, this is the standard definition of State of health (SOH). Generally, for Lithium-ion batteries, the end of life with respect to automotive purposes is approximately when the cell loses 70-80% of its maximum capacity at which point the SOH would be 0%. To accurately measure SOH directly is quite difficult as a qualitative index, so most methods measure related characteristics such as voltage, temperature or current or create a model using previous backlogged data for predictions. The methods are generally categorized into two major categories; Experimental based analysis and model based, where either will break down into further subcategories.

3.2 SOH Estimation Techniques

Accurate information of battery state of health (SOH) is informs the user when the battery should be replaced and also helps to determine whether the battery is useful for second life application or need to be scrapped [71]. SOH is often represented by battery capacity and impedance that is used to evaluate the aging level. However, determining SOH online is highly challenging [72]. Broadly, three types of battery SOH estimation methods are

reported in literature namely, electrochemical impedance spectroscopy (EIS), model-based, and data-driven estimation techniques. In the case of model fit-based technique, capturing the physical, chemical, and materials properties and processes of a battery using a purely electrical model is often not adequate and questionable. Moreover, the prediction accuracy of model-based techniques deviates over time due to battery aging and changes in the battery operating environment. Data-driven machine learning (ML) methods typically require a large volume of high-resolution historical as well as present operational data which is often very challenging to obtain, resulting in reduced prediction accuracy [73], [74]. EIS, commonly known as AC impedance spectroscopy, is an effective electrochemical analytical tool that can analyze the many electrochemical properties of a LIB and utilize them to forecast its state parameters [75], [76]. EIS is also a non-destructive method as imposing AC signal for a short period of time doesn't affect the battery's normal function [75]. Impedance of LIB consists of ohmic resistance, charge transfer resistance, and solid electrolyte interface (SEI) resistance. This can be expressed in the form of complex impedance in the frequency domain which could be further analyzed to estimate SOH [76], [77]. Several SOH estimation techniques have been proposed based on EIS techniques and it is witnessed that impedance measurement-based LIB SOH estimation technique is the most accurate compared to the model-based and ML-based techniques [78], [79].

3.3 Battery Impedance to State of Health Prediction

3.3.1 EIS Equivalent Model of Lithium-ion

The most common method to estimate the state of health of a battery is utilizing electro-impedance spectroscopy to read the cell's internal impedance and resistance. Online measurement of battery impedance requires installing an impedance spectrometer along with onboard BMS. That not only increases the cost and weight of the BMS but also increases the complexity. Therefore, instead of using an impedance spectrum, a novel technique utilizing a single frequency impedance measurement and pre-installation battery impedance data is proposed for online SOH estimation for the practical purpose of BMS. The idea is to first collect the battery impedance at the experimentally obtained best frequency with respect to cycle number before installing the battery in practical application and load the data inside the BMS. Then, during every charging cycle at each 30% SOC,

impose the same frequency AC signal for a few seconds to measure the battery impedance. Finally, compare the measured impedance with the previously stored impedance data to determine SOH using interpolation. The flowchart of the proposed SOH estimation technique is shown in Figure 13.

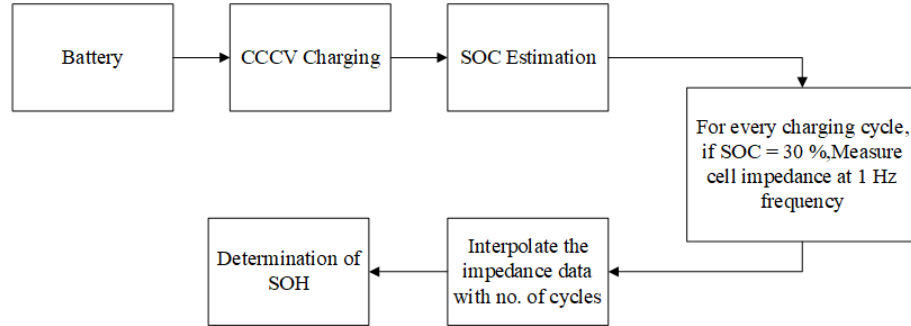


Figure 13 Flowchart of the impedance measurement-based battery SOH estimation scheme

Impedance is calculated by applying a superimposed sinusoidal excitation at a particular frequency (f) and measuring the battery response, which is dependent on the battery impedance [80]. The galvanostatic EIS method [81] is used here for exciting the batteries where a sinusoidal current is superimposed over the DC current (I) of the battery as shown in (8).

$$\Delta I = I_{max} \sin(2\pi ft) \quad (8)$$

The voltage response from the excitation signal can be determined as follows;

$$\Delta V = V_{max} \sin(2\pi ft + \phi) \quad (9)$$

Here, voltage response amplitude (V_{max}) and phase angle (ϕ) are determined by the frequency. The impedance is then given by the following equation,

$$Z(f) = \frac{V_{max}}{I_{max}} e^{j\phi} \quad (10)$$

The electrochemical impedance [$Z(f)$] is a complex number consisting of real and imaginary parts. The impedance is affected by the frequency employed, the magnitude of the voltage and current perturbation, the phase shift between waves, and other factors such as battery SOC, SOH, and temperature [82]. SOH is defined as the ability of the battery to supply or store energy in comparison to its original or ideal circumstances. It is given by the following equation,

$$SOH = \frac{\text{Actual capacity}}{\text{Initial capacity}} \times 100\% \quad (11)$$

$$SOH = \frac{\text{Actual resistance}}{\text{Initial resistance}} \times 100\% \quad (12)$$

The SOH of the arbitrary battery can be estimated by using its internal resistance as follows [83].

$$SOH = \left| \frac{R_{s(selected)} - R_{s(aged)}}{R_{s(fresh)} - R_{s(aged)}} \times 100\% \right| \quad (13)$$

Where $R_{s(selected)}$ is the ohmic resistance of the battery at the test (Ω), $R_{s(aged)}$ is ohmic resistance of the aged battery (Ω), $R_{s(fresh)}$ = The ohmic resistance of the fresh battery (Ω).

The test system used a D&V BCT-150 battery cell tester for the internal modules to assist with EIS. The main components of the system are the Dell precision 3431, battery cyclers, EIS module, and coulombic efficiency. Internally on the Dell precision 3431, the logging system will set the Constant-Current Constant-Voltage (CCCV) cycler profile using the BCT-PRO in conjunction with the cycler configuration and DV Linkviewer will store the data after the first stage of processing on an internal local server. The EIZFAN NCM 18650, 3.6V 2200mAh cylindrical cell is used for testing here. The temperature is kept to approximately room temperature. The galvanostatic EIS measures are followed in this study. The experimental setup and the protocol are shown in Figure 14.

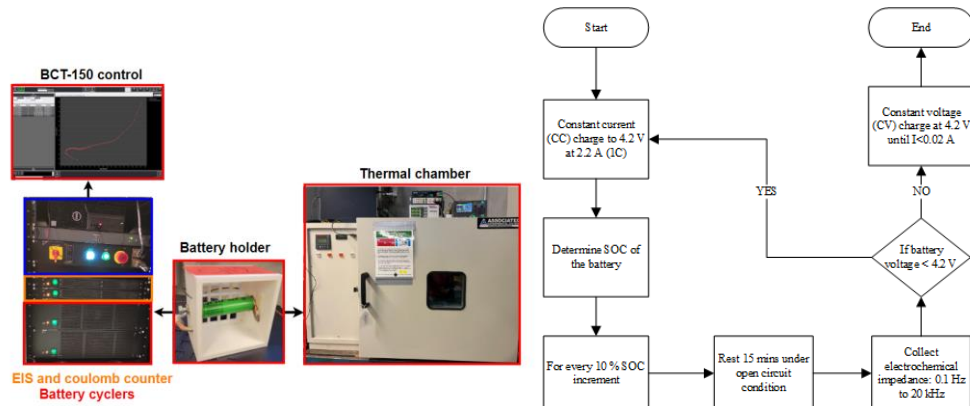


Figure 14 a) D&V BCT-150 Battery Cell Tester and b) the EIS data collection Protocol

3.3.2 Results of Impedance State of Health Estimator

At first, the best suitable frequency for SOH estimation has been determined from the experimental data analysis. The variation of the real part and the imaginary part of the cell impedance with respect to cell SOC is shown in Figure 14 (a) and 14(b) respectively. It can be seen from Figure 14 that both the real and imaginary parts of the LIB cell impedance

are sensitive to the battery SOC. Interestingly, it is evidenced that the variation of both real and imaginary parts of cell impedance is negligible at 30% cell SOC. Therefore, it would be convenient and more accurate if the measured impedance at 30% cell SOC is considered for SOH estimation. Now, another set of experiments is conducted to measure the impedance of cells at 30% SOC with respect to the number of charging cycles. The frequency range of 0.1 Hz to 20 kHz is used for EIS. After detailed analysis, it is noticed that the variation of resultant impedance (2 to 0.5 ohm) of the cell is maximum at 1 Hz over the 200-usage cycle of the battery. Therefore, the interpolation between the two impedance data points will be easier and more accurate for SOH estimation. The variation can be seen in Figure 15(b). Thus, 1 Hz frequency has been considered for impedance measurement for this battery system.

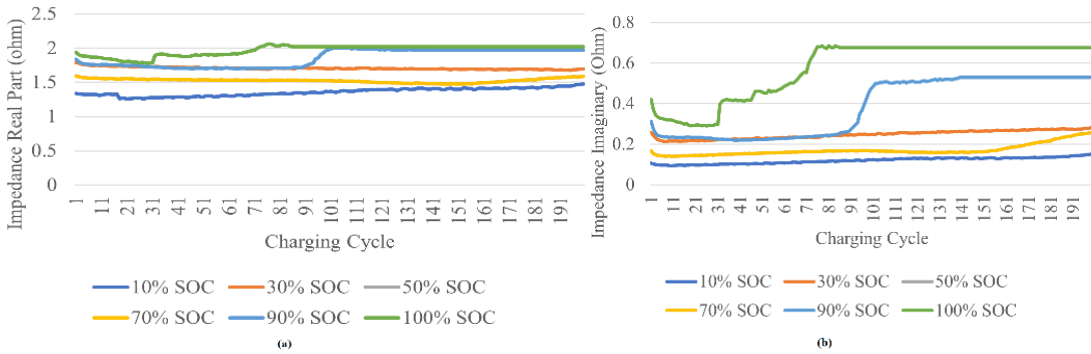


Figure 15 Battery impedance (a) real part (b) imaginary part at a different level of cell SOC and charging cycle

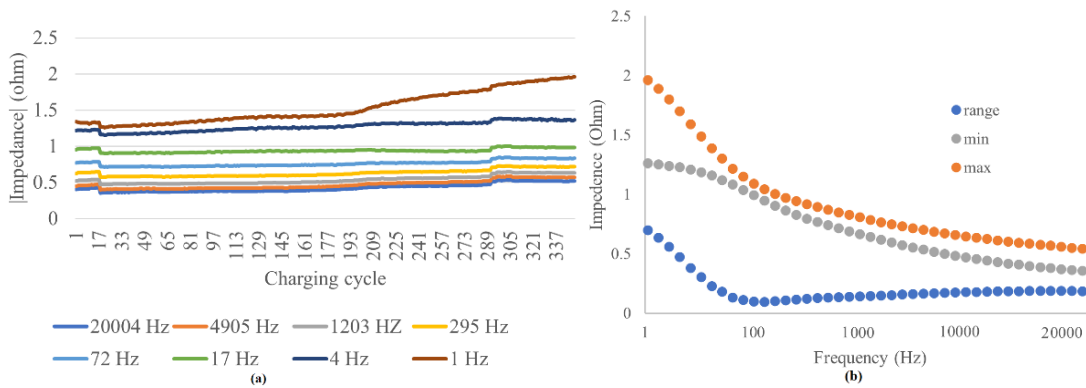


Figure 16 Cell impedance (a) At different frequency and charging cycle (b) Variation of impedance at 1 Hz

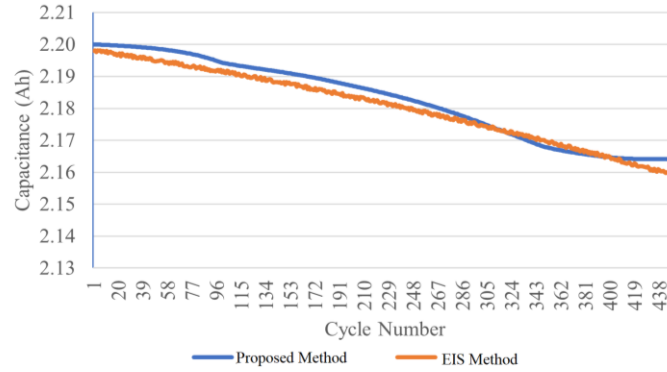


Figure 17 Capacity fade estimation results

Analysis of EIS data revealed that the cell impedances at 30% SOC and 1 Hz frequency are the best representative data points for SOH estimation for this specific cell chemistry. The comparative plot, Figure 17, between capacity fade estimation considering impedance measurement over entire frequency spectrum and capacity fade estimation by the proposed method shows the proposed technique is highly accurate with statistical $R^2 = 0.90$ which is acceptable for all practical purposes of BMS. The primary advantage of the proposed technique is that the EIS does not need to be implemented inside the EV BMS. Only a simple DC/AC converter within the BMS power electronics is required to generate an AC signal of a single frequency at every charging cycle when battery SOC reaches 30% followed by a 10-minute time delay, to obtain a stable state to record the voltage response of the selected current signal. Then the measured impedance will be used to retrieve SOH by comparing the impedance value previously stored in the BMS memory during battery pack testing before installing in EVs. As the proposed method measures the impedance of the battery by looking into the external characteristics thus, in-depth knowledge of LIB chemistry and prior historical usage data is not needed, resulting in a more convenient SOH estimation. This will not only reduce the cost and weight of the BMS but also reduce the complexity of SOH estimation with an acceptable range of accuracy.

3.4 Battery Thermal-SOH Model

3.4.1 Battery Thermal Model to State of Health

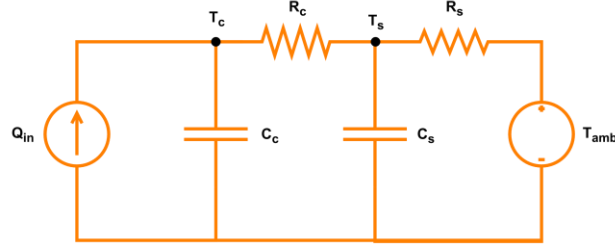


Figure 18 Equivalent thermal model of LIB

The second-order equivalent thermal model (ETM) of LIB, as shown in Figure 18, is chosen as a base model requiring only 2RC pairs, developing the distinction of ranges, either core to surface or surface to ambient. The different parameters used are thermal resistance and thermal capacitance, assigned to their specific region. The major inputs are the constant ambient temperature source and the heat flow from the internal heat losses. In Figure 18, P_{loss} is the battery electrical power loss, T_{amb} is the ambient temperature, C_c is the core thermal capacitance, R_c is the core thermal resistance, C_s is the surface thermal capacitance, R_s is the surface thermal resistance, T_c is the battery core temperature, and T_s is the battery surface temperature. In addition, the battery capacity fade also depends on the usage pattern and operating temperature, such as the discharge current profile [4]. Typical implementations of temperature to SOH relations use heavy models to accurately determine the battery's condition such internal resistance-temperature relation during cycle such as by Lin et al [84]. Other models utilize data driven technique with machine learning such as the Gaussian process regression proposed by Guo et al [85]. The input for the battery thermal model is primarily compiled from the I^2R losses which the overarching system adjusts based on SOH and temperature monitored externally. Therefore, the ETM assumes a homogeneous core material heat transfer and a different heat transfer rate for the surface.

$$Q = K * A * (T_{amb} - T_s) \quad (14)$$

$$P_{loss} = Q_{in} = I^2 * (R_{total}) \quad (15)$$

$$R_{total} = R_0 + R_1 + R_2 + R_{SoH} + R_{temp} \quad (16)$$

$$C_c \frac{dT_c}{dt} = P_{loss} - \frac{T_c - T_s}{R_c} \quad (17)$$

$$C_s \frac{dT_s}{dt} = \frac{T_c - T_s}{R_c} - \frac{T_s - T_{amb}}{R_s} \quad (18)$$

Where Q is the heat flow, A is the surface area of the battery, T_c , T_s and T_{amb} are the core, surface and ambient temperature of the system, K is the heat transfer coefficient, and R_{total} is the summation of internal DC resistance R_0 , and internal transient resistances (R_1 , R_2). Here the value of Q can be calculated using equivalent electrical circuit model for further utilization in ETM as demonstrated in [5], [6]. The heat flow here is considered as convection and not radiation or conduction, as the battery is suspended and the ambient temperature is controlled. The key variables considered are the specific heat transfer coefficient of the battery. The secondary surface RC pair will make a more significant contribution since it can give some instances for conversion from the thermal model to the electrical characterization model with a found polynomial function as in (19) and (20). Figure 18 shows the equivalent thermal model considering battery aging and temperature.

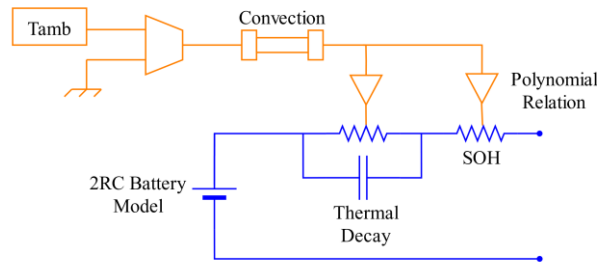


Figure 19 thermal model considering battery aging and temperature

3.4.2 Thermal-SOH Results

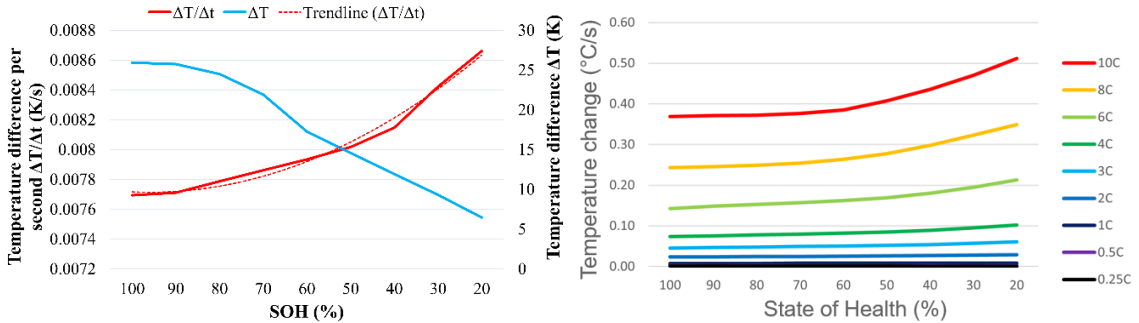


Figure 20 For 25 degrees Celsius (a) Relation between temperature difference per second and temperature difference with SOH (b) Normalized temperature change for different C rates

The temperature difference and the temperature differential are shown in Figure 20(a). The trendline line is to interpolate the SOH based on surface temperature. Taken at face value, the temperature difference decreases with lower SOH cell. This is poorly represented since it does not consider that the run time for lower SOH cells is shortened as minimum voltage is reached sooner. To account for this, the overall temperature rise is taken over the total time giving a better representation. This now shows that the temperature rise is increasing in relation to the degradation of the cell. The experiment was run again for different C-rate on new cells as shown in Figure 20 (b), which mostly just demonstrated a larger correlation of degradation between the overall temperature rise to the SOH of battery.

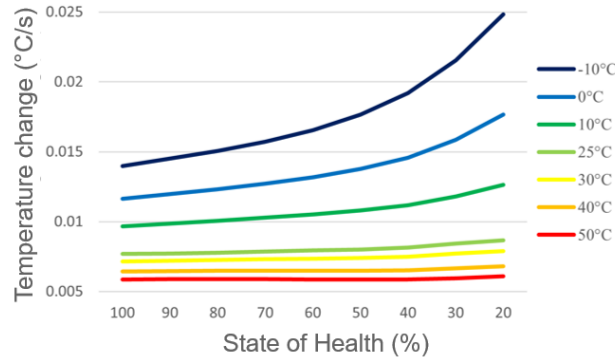


Figure 21 For 1C SOH and temperature rise at different starting temperatures

$$\Delta T_{rise} = 2E - 05(SOH)^2 - 4E - 05(SOH) + 0.0077 \quad (19)$$

$$IR = 0.0046(SOH) + 0.0167 \text{ [Ohm]} \quad (20)$$

The internal resistances of the batteries are also measured periodically with comparison to the SOH as the median for the temperature increase rate as shown in Figure 22(a). The relation fairly correlates linearly with estimating the internal resistance growth to the nominalized temperature rise. The time taken for discharge with the changes in SOH of the battery at a nominal level as shown in Figure 22(b), shows a relatively linear relationship between the discharge time decrease and the decrease of the SOH, except between 100% and 90% SOH where the discharge time is relatively the same. Hence the internal resistance increases, and the temperature rise does not greatly affect the total capacity until after the cell falls below 90% SOH.

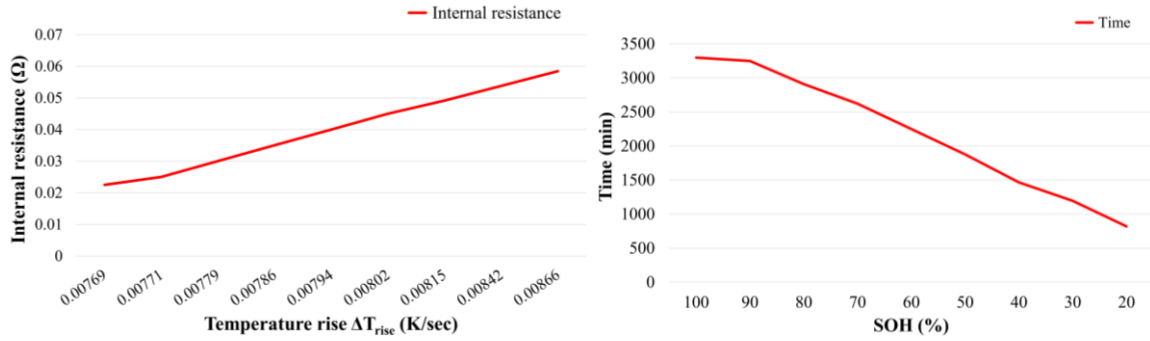


Figure 22 (a) Internal resistance vs. temperature rise and (b) Time taken to discharge per SOH

3.5 Summary

Critical analysis of EIS data revealed that the cell impedances at 30% SOC and 1 Hz frequency are the best representative data points for SOH estimation for this specific cell chemistry. The comparative study between capacity fade estimation considering impedance measurement over entire frequency spectrum and capacity fade estimation by the proposed method shows the proposed technique is highly accurate with statistical $R_2 = 0.90$ which is acceptable for all practical purposes of BMS. The primary advantage of the proposed technique is that the EIS does not need to be implemented inside the EV BMS. Only a simple DC/AC converter within the BMS power electronics is required to generate an AC pulse of a single 1 Hz frequency at every charging cycle when battery SOC reached 30% followed by a 10-minute time delay, to obtain a steady state, to record the voltage response of the selected 1 Hz current signal.

With an alternate method of SOH estimation, the differential temperatures between new and aged cells are used as a health indicator for SOH estimation. The cells tested at room temperature with 1 C rate discharge rate for establishing the mapping relationship and validation of the proposed concept. The estimation showed a non-linear increase in temperature difference of about 0.001°C over the range of 80% SOH drop.

Chapter 4. Hybrid Battery Development

As mentioned, all BMS will have a form of equalization implemented, therefore, to select the topology that will be the most suitable for BMS development in the future a comparison study of three different balancers will be performed. The selected balancers will be the industrial standard passive balancer, a proposed active cell-to-pack-to-cell with supercapacitor and the hybrid balancer. To assess the performance benefits of the different battery balancer, three topologies were made in Simulink for analysis.

4.1 Initial Conditions

The selected cell for analysis and simulation modeling will be based on the Samsung 40T INR21700 due to higher performance characteristics and ease of acquisition from the Ontario Tech Racing team. The battery features very high discharge characteristics suitable for short duration racing or needs for high instantaneous power.

Table 2 Nameplate Information of Samsung 40T INR21700 LIB Cell

Property	Value
Nominal Capacity	4000 mAh
Continuous Discharge Rating (max)	35A
Nominal Voltage	3.6V
Maximum Voltage	4.2V
Discharge cut-off Voltage	2.5V
Discharge cut-off SOC	30%
Nominal discharge	1C (4A), 45A max
Nominal charge	0.5C (2A), 1.5C (6A) max, 100mA cut-off

To ensure testing homogeneity between the different tests, the basic test parameters were kept the same with a charge and discharge of 1C (4A) utilizing a CCCV charging algorithm and an ambient 20°C. All the simulated cells between the tests had the same starting variation between the cells of 20% SOC difference. The cells are also limited from discharging below 30% SOC to avoid going over the knee.

Table 3 Starting State of Charges for charge and discharge

Cell number	Starting SOC for charge (%)	Starting SOC for discharge (%)
1	40	100
2	36	93
3	27	87
4	20	80

4.2 Experimental Setup

The system would operate with the OPAL-RT OP4510 hardware-in-loop simulator and OP8665 digital signal processing board. The utilization of OPAL-RT products is to assist in rapid simulation and prototyping of hardware utilizing the same control system. The OP4150 would function as the simulation of the hardware while setup was ongoing and OP8665 would be utilized as the controller of the simulated hardware. Once system fabrication would be completed the OP8665 could then be utilized as the controller as TI TMDSCNCD28335 which houses the C2000 microcontroller.

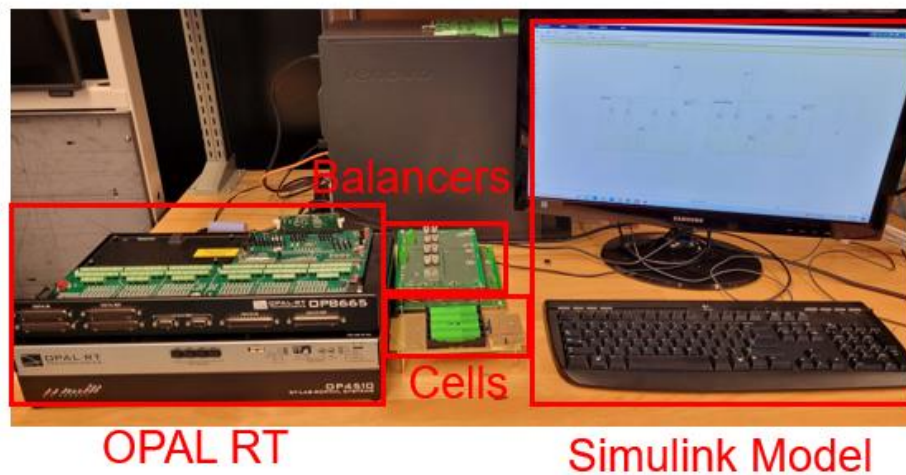


Figure 23 Hardware setup

4.4 Passive Balancer

For comparison purposes, the industrial standard resistive balancing will be used as the benchmark. Utilizing the passive balancing topology shown in Figure 5 Passive equalizer, the topology clearly shows the lowest part count of any balancing topology while also utilizing the cheapest components. Spreading the initial SOC states between 20-40% for a deeply unbalanced pack as a setpoint for all the topologies will assist in the comparison. Utilizing a nominal bleed resistor value of $15\ \Omega$, the balancing current is nominally 280 mA. as higher resistance bleed resistor would need longer time to balance, and a lower resistance would incur higher losses.

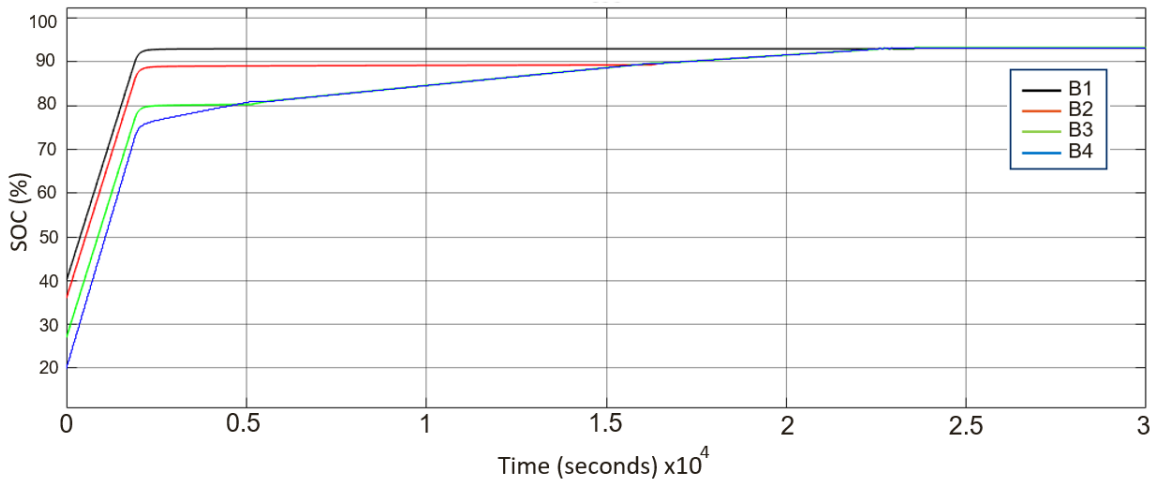


Figure 24 SOC of passive balancing

As is show in Figure 24 SOC of passive balancing, passive balancer can balance the cell, but the time taken is very high and would severely limit acceptable charge times. The topology is most clearly adjusting the charge rates of the batteries in CV mode when the current is already throttled, which reduces the effectiveness of balancing by requiring more time to charge. Since passive balancers essentially prevent the highest SOC cell from reaching the maximum safe voltage, other cells that need to be charged or balanced are greatly limited. To achieve an overall SOC difference of 1% the charge time is around 21800 seconds which is far too long for reasonable charging, and therefore is only recommended for battery idling or charge balancing.

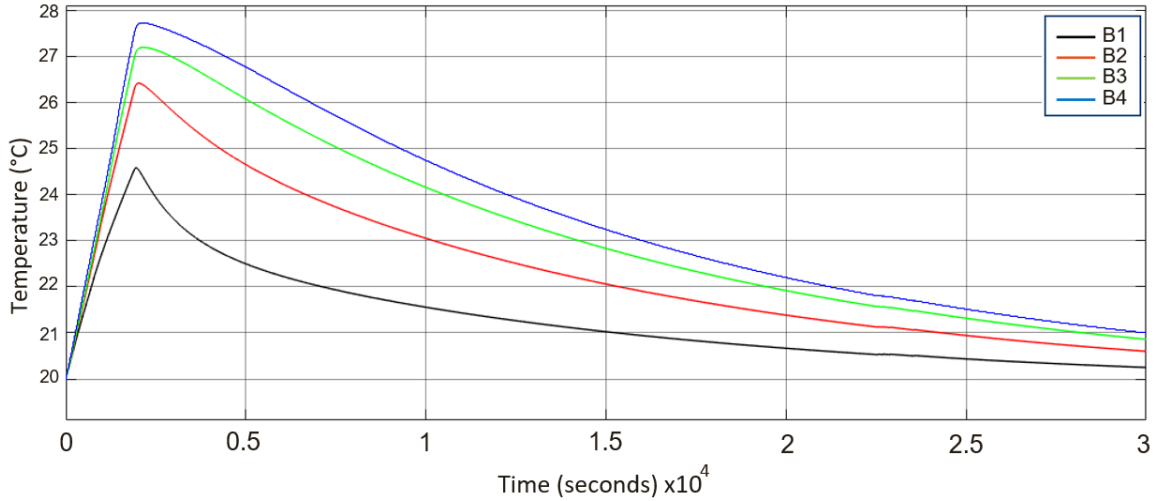


Figure 25 Temperature of passive balancing

In Figure 25, the graph demonstrates the low heat generation through the entire charge time for passive balancing. B4 experiences the most heat generation as it has the full 1C charge during the entire CC range while the batteries with more starting charge receive less current and generate less heat. The long CV section allows for cooling almost back to 20°C, but the timing is far too long for any effective balancing or charge. As shown in Figure 26, the batteries are only charging in CC for 1866 s and then is in CV for the rest of the duration.

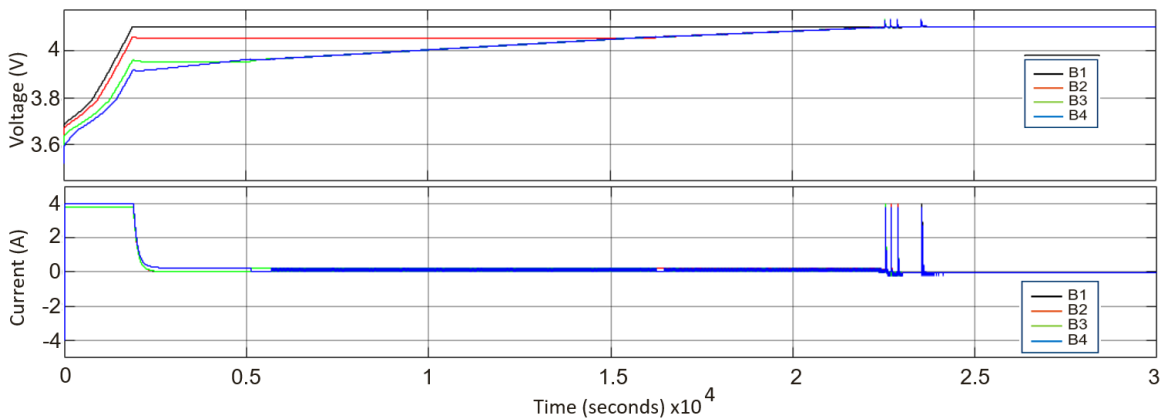


Figure 26 Voltage and current of passive balancing

4.5 Active Balancer

One development combines a supercapacitor (SC) and bidirectional DC-DC converter to create a C2P2C active balancing scheme with fewer active switches and greatly increased balancing speed by maximizing for power transfer per duty cycle. The SC helps to shuttle

more balancing energy in a single cycle enabling the use of low balancing frequency resulting in low switching losses. The DC-DC converter works in buck-boost mode to control the charging/discharging voltage of the SC resulting in improved balancing speed irrespective of individual cell voltage level. Lastly, conventional switched capacitor-based methods need to use high frequency to enhance balancing speed which reduces efficiency and accuracy due to low energy storage capability. Comparatively, a supercapacitor has a much higher energy storage capacity allowing for the low frequency of operation resulting in reduced switching loss, improved efficiency, and cycle life and greatly enhancing the reliability [86].

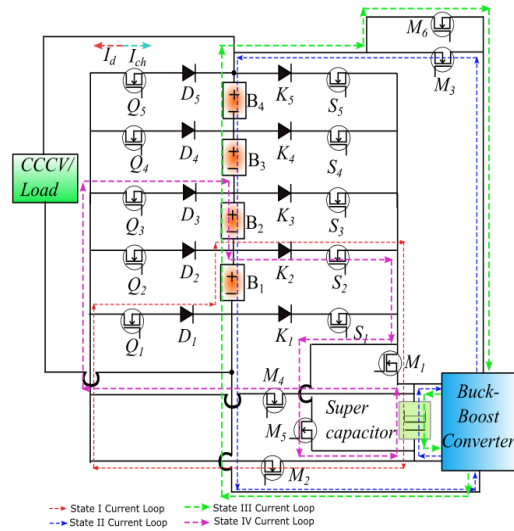


Figure 27 C2P2C with super capacitor balancer

The balancing network consists of one SC, one ideal bidirectional DC-DC converter, and six (M_1 - M_6) power switches. The SC is used as a temporary energy tank while shuttling the balancing energy and the voltage is modulated by the DC-DC converter. The switches M_1 to M_6 that access the SC and direct the flow of balancing energy, are independent of the number of series-connected cells. The power rating of these switches depends on the pack voltage, balancing current, and operating frequency. A constant current constant voltage (CCCV) charger and a constant current load as shown in Figure 27 are also connected externally for charging and discharging the LIB pack.

Table 4 list of active switches during charging and balancing

Balancing During Charging Period			
B ₁ =Most charged cell		Generalized case when n th cell = most charged cell	
State I	State II	State I	State II
Q ₁ , S ₂ , M ₁ , M ₂	M ₃	Q _n , S _{n+1} , M ₁ , M ₂	M ₃

Table 5 List of active switches during Discharging and balancing

Balancing During Discharging Period			
B ₂ =Least charged cell		Generalized case when n th cell = least charged cell	
State III	State IV	State III	State IV
M ₆	Q ₃ , S ₂ , M ₅ , M ₄	M ₆	Q _{n+1} , S _n , M ₅ , M ₄

During battery pack charging, C2P balancing is performed whereas during discharging P2C balancing is performed. Starting with charge balancing, (state I), excess energy is transferred from the highest SOC cell to the supercapacitor. The stored charge is then transferred to the entire battery pack through the DC-DC converter in boost mode (state II). For discharge, the SC is charged from the battery pack through the DC-DC converter in buck mode (state III), followed by the release of the stored energy to the lowest SOC cell (state IV). The duty ratio of State I and state II is considered 66%, and the switching frequency is $f = 1$ Hz. Whereas reverse ratio is considered for State III and State IV. In both cases, the DC-DC converter operates in discontinuous current conduction mode to avoid saturation of the supercapacitor and to reduce stress on power switches. The duty and frequency of the operation are judiciously chosen to ensure almost zero initial charges before starting state I and sufficiently charged at the beginning of state III. Individual cell SOC is used to determine the most and least charged cells. The list of active switches when B₁ is the most charged cell during charging and B₂ is the least charged cell during discharging along with generalized statements are given in Table 4 and Table 5 respectively. The control flow chart is in appendix B.

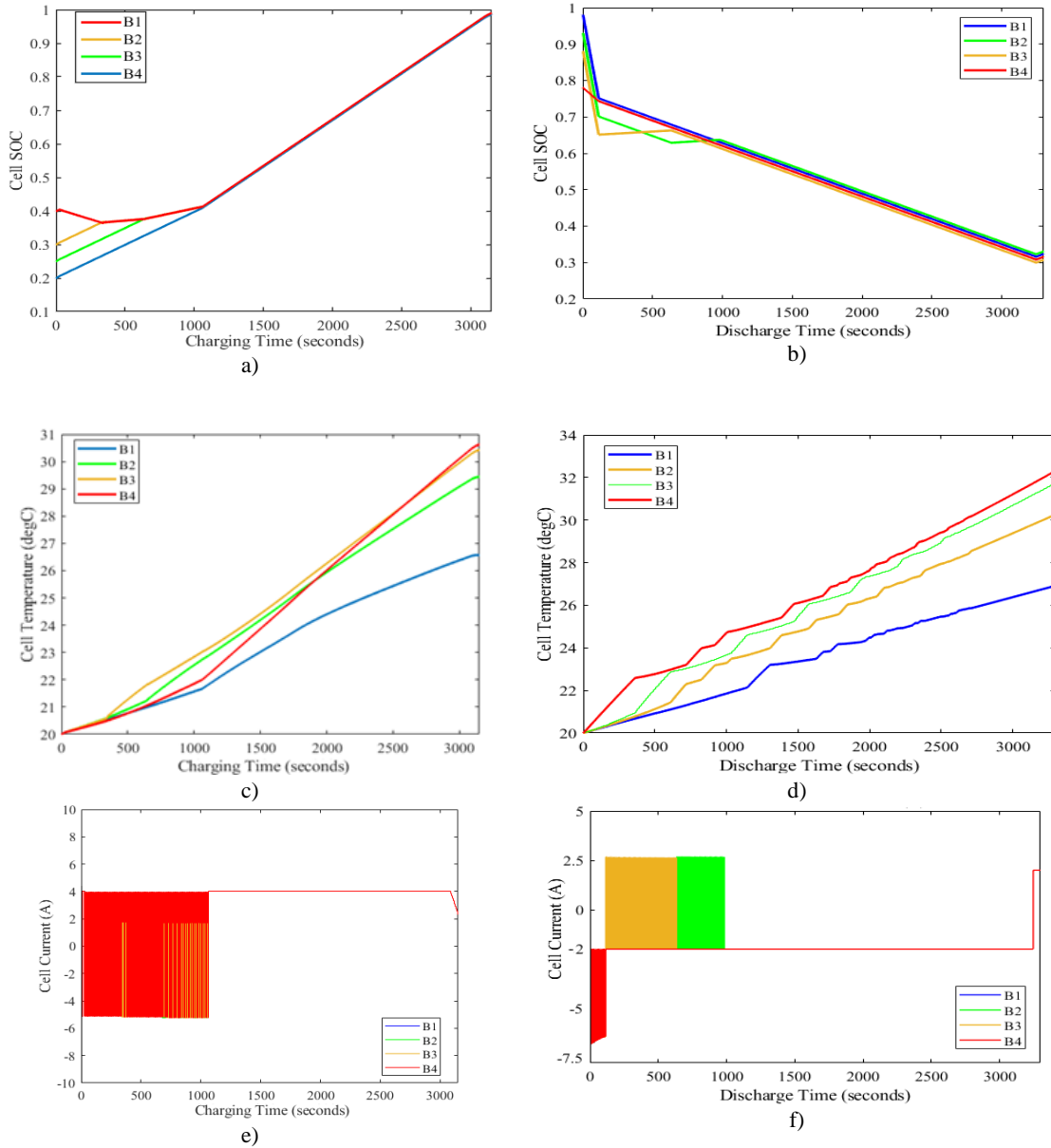


Figure 28 Balancing performance of the super capacitor balancer during (a) charging SOC, (b) discharging period SOC, (c) charging cell temperatures, (d) discharge cell temperatures

The charging operation started with different initial SOC and slowly approached each other simultaneously with the progress of battery pack charging confirming the operation of C2P balancing. At around $t = 1060$ seconds the balancing operation ended as all cell SOC's convergent to threshold ($\Delta\text{SOC} = 1\%$) from the initial SOC imbalance of 20% (max). This is confirmed by the current plot (Figure 28(f)) showing no over correction after $t=1060$ seconds, only a constant 4A charging current is drawn by the battery pack. Similarly, the balancing results during the discharging period with the initial SOC variation of 20% are

shown in (Figure 28 (b)). Evidence of constant discharge current of 2 A and no stress of balancing current at around $t = 988$ second confirms the effectiveness of P2C balancing during discharge. The charge imbalances are reduced from 20% (max) to 1% (ΔSOC) in this period. The estimation does have overshoot where the B3 and B2 fall below and outside the expected range but are quickly assisted back with the desired SOC at around 1000s.

4.6 Hybrid Balancer Design

A hybrid dual-stage cell-to-pack (C2P) balancing strategy is proposed by in this thesis that takes advantage of both active and passive balancing. The hybrid balancing topology is shown in Figure 29.

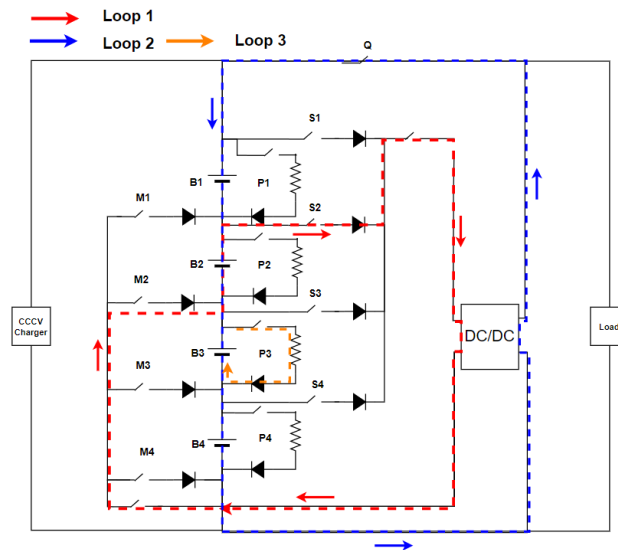


Figure 29 Hybrid C2P and passive cell balancing topology

The balancing topology shown in Figure 29 demonstrated uses a balancing topology for four series-connected cells ($B_1 - B_4$) in the string. The system currently utilizes three MOSFETs and diodes per cell, which are grouped into $Q_1 - Q_4$ and $S_1 - S_4$ for the active balance topology and $P_1 - P_4$ for passive balancing. The power diodes per switch are to ensure unidirectional power flow and avoid circulation current. The DC/DC converter is connected using M1 and M2 by either connecting the system from the pack side or from the cell access network. The DC/DC converter itself is utilizing a unidirectional flyback boost converter. The system runs in two modes during charging. For lower SOC and initial charging, the active cell-to-pack balancing system uses M_n and S_n MOSFETs to

link the highest SOC cell to the flyback converter in loop 1. The secondary loop converts the initial input voltage to the pack voltage where ‘n’ would be the desired boost ratio. The excess energy is then boosted and linked to the pack to momentarily assist the charger to redistribute the energy to the whole pack. At higher SOC values during charging, during CV, and idle mode, the second passive balancing is activated. During discharge, the system would only utilize the active cell balancing capabilities as shown in Figure 29.

4.6.1 Balancer Control

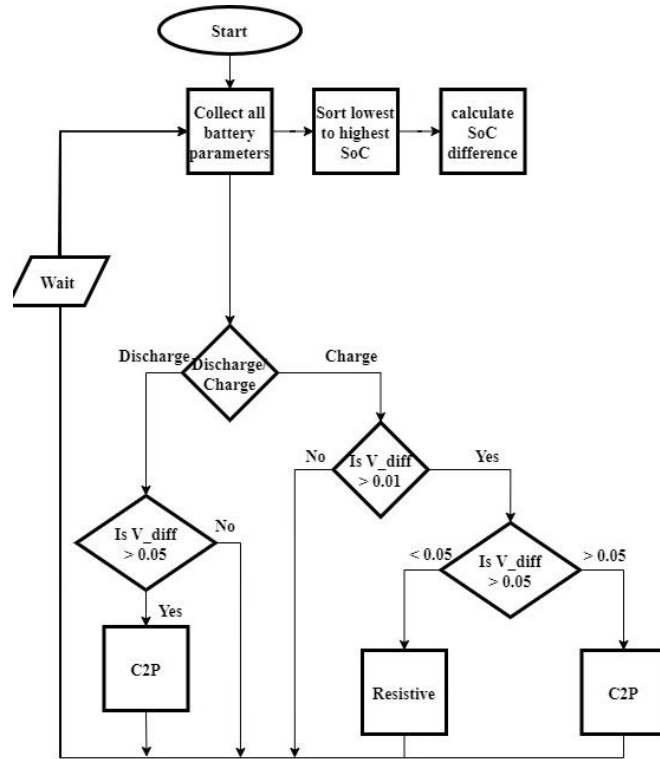


Figure 30 hybrid balancing algorithm

The control decision starts with collection of all cell’s states and current parameters and then the cells are sorted from highest to lowest voltage. After checking the current charge or discharge cycle, the balancer will then calculate the current voltage difference and pick if balancing is needed. If balancing is needed, the control will then select the appropriate balancing method based on the voltage difference. The control system is simulated within the MATLAB Stateflow to keep track of the different paired MOSFET states to control each loop and the battery. The state functionality of the active and passive balancer is listed in Table 6.

Table 6 list of active switches during charging and balancing

Balancing States				
Charge			Discharge	
Loop 1	Loop 2	Loop 3	Loop 1	Loop 2
M ₁ , S ₁	Q	P ₁ , P ₂ , P ₃	M ₁ , S ₁	Q

4.6.2 Continuous Conduction and Discontinuous Conduction Modes

Since the flyback converter can be operated within two modes discontinuous conduction mode (DCM) and continuous conduction mode (CCM), determination of which mode would be better suited to the application must be done. Since this is a low power operation due to the high voltage boost and ease of implementation is one of the primary performance targets CCM can be utilized. With CCM, the benefits can be exploited such as lower peak switching currents, reduction of EMI and lower coupled capacitor size, but the drawbacks such as higher ripple must be compensated. The duty ratio for the DC/DC MOSFET is 0.5 which is standard to allow for CCM. The overall operating frequency is 1 kHz.

4.6.3 DC/DC Converter Design

Isolation is necessary to allow the battery to reference the negative terminal for a closed loop. If a non-isolated DC/DC converter is used for a pack related balancer, the batteries may need to reference the overall ground of the pack producing extremely different balancing rate per cell. For inclusion for an isolation device, the optimal solution would be to reduce the number of devices as much as possible to reduce weight as opposed to each cell having individual transformers. Of the basic boost topologies, flyback converters are less complicated compared to a forward converter which would require a three-winding transformer and more switching requirements. For these reasons, flyback converters have been previously utilized for battery balancing in addition to cost reduction and good efficiency [12], [73]. These topologies have been analyzed for low cell variation, long equalization time or balance the batteries during a static timeframe with no active charge or discharge.

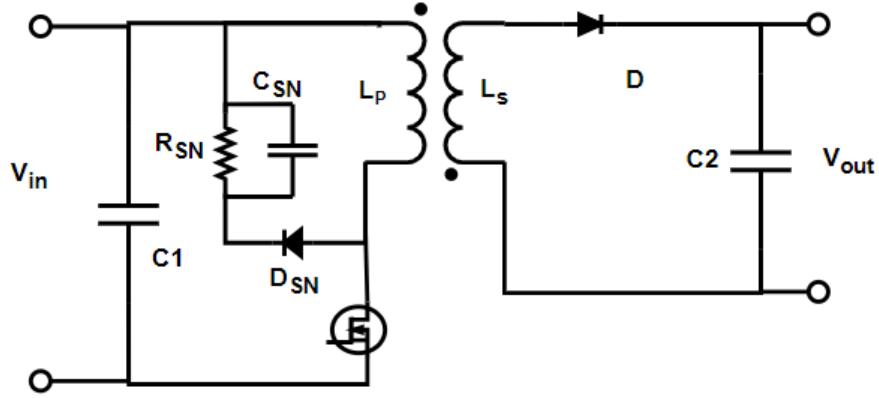


Figure 31 Flyback converter

For the flyback converter value calculation, the design requirement utilizing a maximum voltage ripple of 50mV to reduce overcharge damage after 4.2V. The maximum current ripple is set for 2% due to the higher voltage for faster cell balancing. The needed voltage out of the system needs to account for the voltage drop from the diode as well as the 1:4 boost needed; therefore, “b” is the number of series cells in the equalizer and V_D is the output diode.

$$V_{out} = b * V_{in} + V_D \quad (21)$$

Calculation of the flyback converter are shown below for equation (22)-(27), where D is the duty cycle, n_{s1} is the turn ratio for the worst-case scenario, C_{out} is the secondary/output capacitor, and L_{crit} is the inductance of the primary side. The lowest considered voltage is 2.5V which is the cut-off voltage of the battery.

$$\frac{n_2}{n_1} = \frac{V_{out} + V_D}{V_{in_min}} * \frac{(1 - D_{max})}{D_{max}} \quad (22)$$

$$n_{s1} = \frac{V_{in_max} * D_{max}}{(1 - D_{max}) * (V_{out} * V_D)} \quad (23)$$

$$L_{crit} = \frac{D_{max}^2 * V_{out}^2 * n}{2 * f * P_{out}} \quad (24)$$

$$I_{p,peak} = \frac{D_{DC/DC} * (\sum v_{in} + v_c)}{2 * L_m * f} + \frac{V_{in_max} * D_{max}}{(1 - D_{max}) * (V_{out} + V_D)} \quad (25)$$

$$I_{s,peak} = I_{p,peak} / \frac{n_2}{n_1} \quad (26)$$

$$C_{out} = \frac{1-D}{8*L*\left(\frac{\Delta V_o}{V_o}\right)^2 * f^2} \quad (27)$$

To follow equation (22), $D_{DC/DC}$ is typically 0.5, so the ratio for $n_1:n_2$ will be greater than 1:8, with a $10*L_{crit}$ the taken coil inductance would be 4.7 nH or larger, and the output capacitance is 0.25 nF based on a frequency of 1 kHz. The max current on the secondary side is 0.5 A. For MOSFET and diode sizing, I_{D_pk} is the maximum current needed to withstand and V_{DS_max} is the maximum voltage which will have a 20% safety factor included after calculation. After calculations and since this part was available in the laboratory, RFP12N10L was deemed suitable for the balancer with a maximum of 30V, 5A maximum rating. Power dissipated in snubbers came to be 0.26W, the peak current rating was larger than 6.5A with safety factor and the maximum voltage for the MOSFET and diode was 3.7V and 34V respectively, which the RFP12N10L and SB2060 is well suited.

$$I_{M_pk} = \frac{P_{in}}{D_{max}*V_{in_max}} + \frac{D_{max}*V_{in_min}}{2*L*f} \quad (28)$$

$$V_{DS_max} = V_{in_max} + \frac{D_{max}*V_{in_max}}{1-D_{max}} \quad (29)$$

$$V_{D_pk} = V_{in_max} + \frac{V_{in_min}}{n} \quad (30)$$

To reduce ringing due to the MOSFET switching off, a snubber circuit is also implemented, and design calculated below in equation (22)-(25). The values from the snubber calculated need a minimum voltage of 3.17 V, power loss of 0.014 W, $R_{snubber}$ needed to be 3510 Ω and a $C_{snubber}$ capacitance of 0.7 μ F and the peak voltage of 8.04 V.

$$P_{snubber} = \frac{I_{peak}^2 * L_{leak} * f}{2} \quad (31)$$

$$R_{snubber} = \frac{V_C^2_{max}}{P_{snubber}} \quad (32)$$

$$C_{snubber} = \frac{1}{R_{snubber} * f * \Delta V_c} \quad (33)$$

$$V_{D_snubber} = 1.2 * V_{DS_max} \quad (34)$$

Coulomb counting was used for monitoring the voltage to achieve cell balancing. The specifications of the DC/DC converter are derived from (28) to (34). The total duration of time of one balancing cycle is $T = t_1 + t_2$ and the frequency $f = 1$ kHz.

In discharge balancing, the C2P will utilize the excess energy from the highest SOC cell to load share with the rest of the pack. The hybrid would primarily only use the active balancer since the passive balancer would introduce heat into the system and greater power losses than expected. The highest SOC cell shuttles the excess power to the converter to assist the pack with load distribution. In this case, the cell would experience double rate discharge, the first would be the regular load from the direct load and an equivalent draw to the DC/DC which the secondary side would have the same demands.

4.6.5 System Efficiency

Since the small incremental power transfer is the main mode of charge delivery all inefficiencies and losses must be accounted for to ensure the efficiency is effective. As the most prevalent component, the MOSFETs play a large part in losses. Utilizing the equations below and the values of the RFP12N10L, the losses per MOSFET in line were found to be 0.05 W per switch.

$$P_{mosfet} = P_{on-h} + P_{on-l} + P_{switching} + P_{Dead\ time} + P_{IC} + P_{gate} \quad (35)$$

$$P_{on-h} = I_o^2 * R_{on} * \left(\frac{V_{out}}{V_{in}}\right) \quad (36)$$

$$P_{Dead\ time} = V_D * I_o * (t_{rise} + t_{fall}) * f_{sw} \quad (37)$$

$$P_{Gate} = (Q_H + Q_L) * V_{gate\ drive} * f_{sw} \quad (38)$$

$$P_{IC} = V_{in} * I_{consumption} \quad (39)$$

Here P_{mosfet} = total power losses through the MOSFET, P_{on-l}/P_{on-h} = low/high side conduction loss caused by MOSFET on-resistance, $P_{dead\ time}$ = dead time loss, P_{IC} = operating loss caused by IC control circuit, P_{gate} = MOSFET gate charge loss, I_o = output current, and R_o = MOSFET on resistance. For the coupled inductor/transformer losses, the calculations were assuming an internal resistance of 0.001 Ω for both the primary and secondary side inductor. The losses from the primary coil secondary coil combined were

0.02W. The total power losses were calculated with equations (35)-(43) and came to be peak loss of 0.4W.

$$I_{pk_rms} = I_{pk} * \sqrt{\frac{D_{rms}}{3}} \quad (40)$$

$$P_p = P_s = I_{rms}^2 * R_{winding} \quad (41)$$

$$P_{total} = 3(P_{D_forward} + P_{mosfet}) + P_s + P_p + P_{snubber} \quad (42)$$

$$\eta = \frac{1}{1+(P_{total}/P_{out})} * 100\% \quad (43)$$

I_{pk_rms} = total power losses through the MOSFET, $P_p/P_s =$, $P_{switching} =$, $R_{winding} =$, η = system efficiency. The output power from the DC/DC converter is nominally 3.8 W with an estimated 83% efficiency.

4.6.6 Simulation Results and Discussion

The simulation software that was used is Simulink specialized power system block to allow for future compatibility with other software such as OPAL-RT HIL and LABVIEW. The simulation tool is ideal since it is easy to utilize, has set modules to input values for all components, and is compatible with battery model structure.

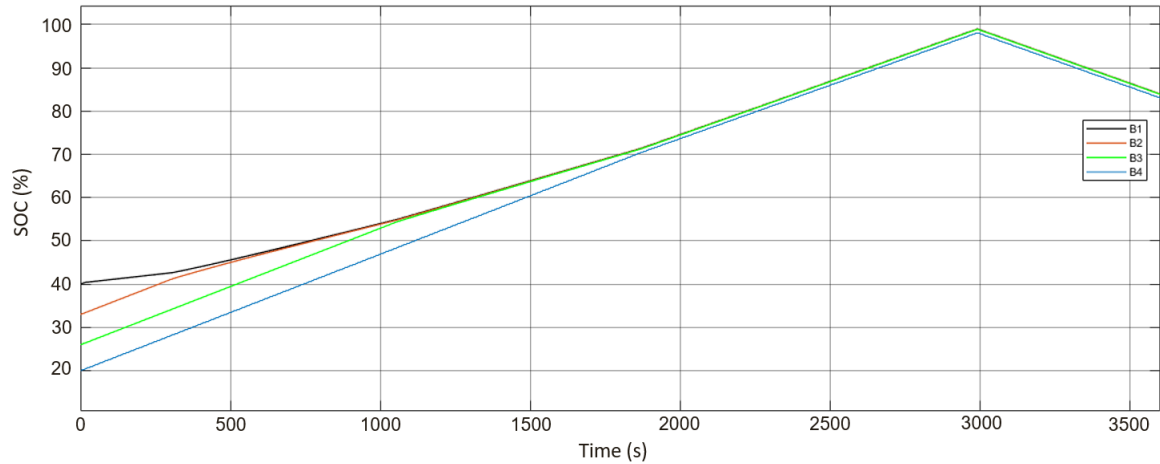


Figure 32. SOC during charging

The hybrid balancer operates both passive and active balancing situationally dependent on the limitations and health conditions. The active balancing between 50 seconds to 1870 seconds would be considered the bulk/coarse equalization reducing the SOC variation greatly from 20% to lower than 5% Δ SOC. The passive balancer can be utilized again if

the SOC is required to be lowered to 1%, reducing the switching requirements of the system and more accurate small variation balancing.

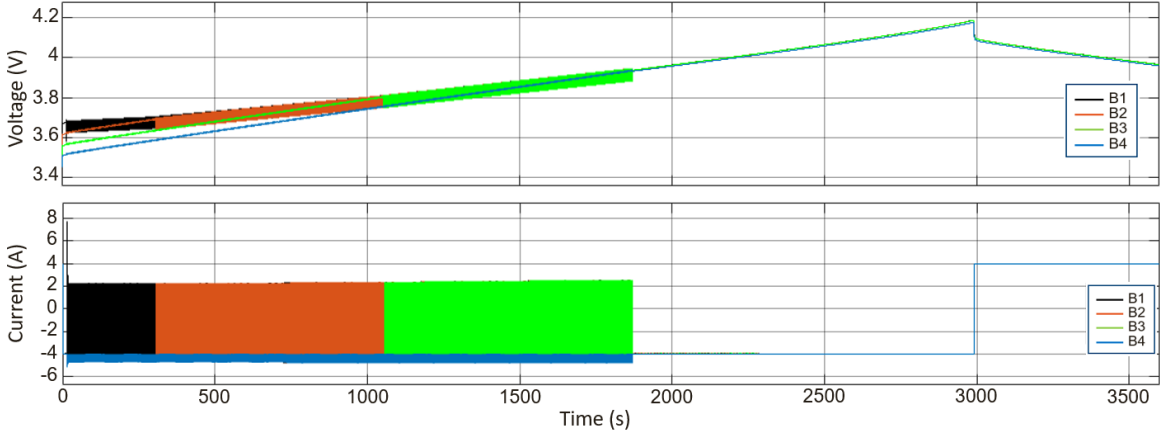


Figure 33 Battery current during charge

The ripple is acceptable with a small operating frequency during the balancing period, staying within the 0.1 V maximum voltage cycle adjustment during the charge. After the bulk equalization ends at 1870s, it is easier to visualize in Figure 33 that passive balancing takes place from 1870s to 2295s to further reduce the cell variation down to 1%. To fully charge up to 4.2 V, the system avoids utilizing CV, reducing the time needed to charge. The ripple currents are high at around 1C as the coupled primary inductor fully charges and discharges within one cycle. Figure 33 show a clear difference in charge rates between the cells, the higher SOC cell experienced a slight rate decrease to around 3.2 A while the lower SOC cells would continuously have a higher rate of charge. For the Samsung 40T, this is acceptable since the maximum allowable charge is 6 A.

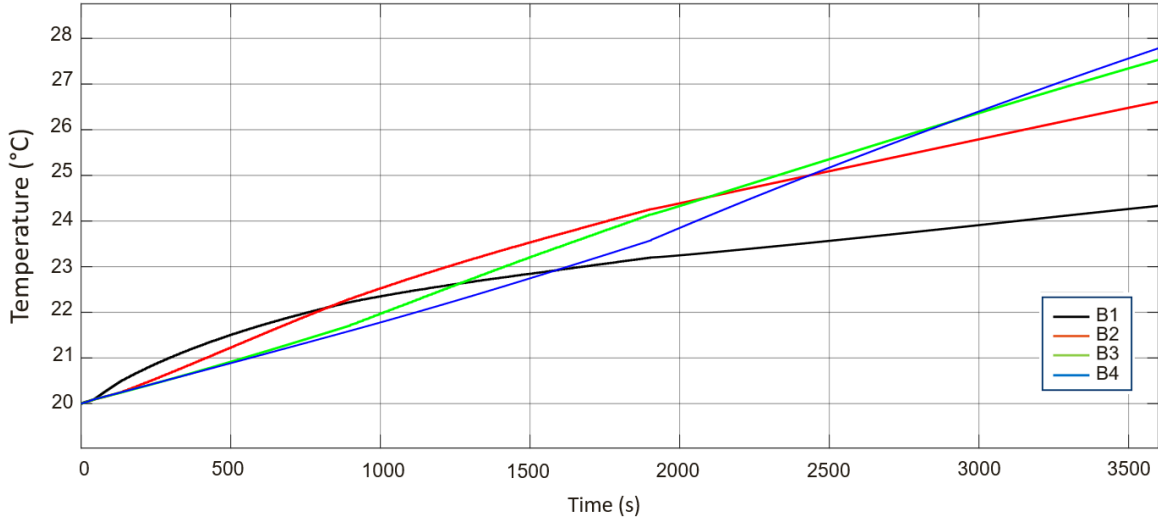


Figure 34 Cell temperature during charging

Overall, the maximum heat generation of the cells only increases by 7.8°C over the entire duration of the charging process, with most of the heat generation during initial start-up and active balancing. During passive balancing the heat generation greatly slows allowing for some cooling, the slowest heat generation period is during CV but since that period is low charge and long duration, it is not ideal for heat reduction during quick charging. The cell with higher balancing cycles experienced the least temperature rise but does still contribute to greatly assist the other cells to charge. Figure 34 also corroborates with the cell currents that the higher cell had reduced CC and therefore experienced reduced temperature rise.

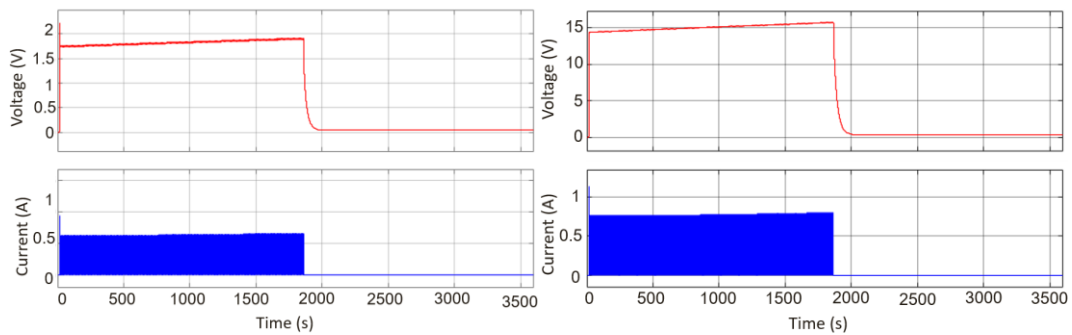


Figure 35 Charge DC/DC input (left) and DC/DC output (right)

Due to the snubber circuit and the input capacitor, the input to the coupled inductor is slightly lower than expected at around 1.75 V and was clamped under 3 V, but this does not change the functionality of the DC/DC converter as it still boosts the voltage to $4 \cdot V_{\text{cell}} + V_{\text{D}}$ and keeps the approximate 4W output. The DC/DC itself stops functioning at

1850 seconds and the input and output capacitors release any stored energy which is relatively decayed.

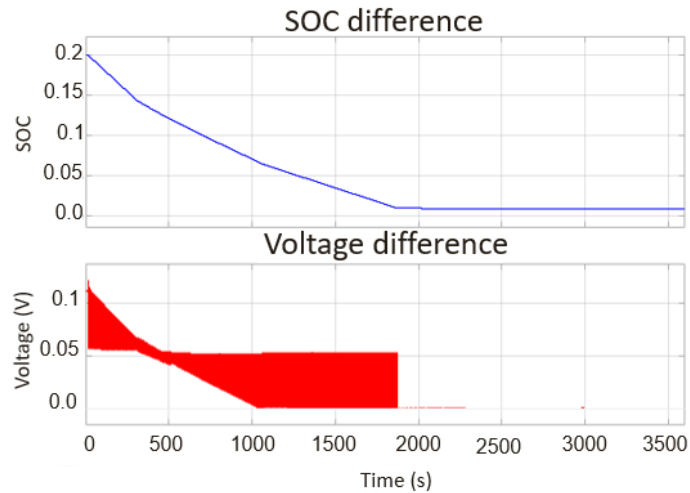


Figure 36 Charge SOC difference, voltage difference

Figure 36 demonstrates the easier to track nature of SOC even when the balancing algorithm is voltage based. Voltage balancing is still preferred as Figure 32 and Figure 36 show there is no overshoot as the cells smoothly consolidate. The balancer brings the SOC difference from 20% down to around 2%, then the passive balancer takes over to reduce switching that may cause over balancing of the top cells.

For discharge, the bulk discharge balancing only takes around 1850 seconds to balance the cells as show in Figure 37. The time taken assist the batteries from sudden load shifts as well as reducing over balancing the cells. The balancing cycle takes 2150 seconds to discharge the cells to 30% balance the cells before changing to charging the batteries.

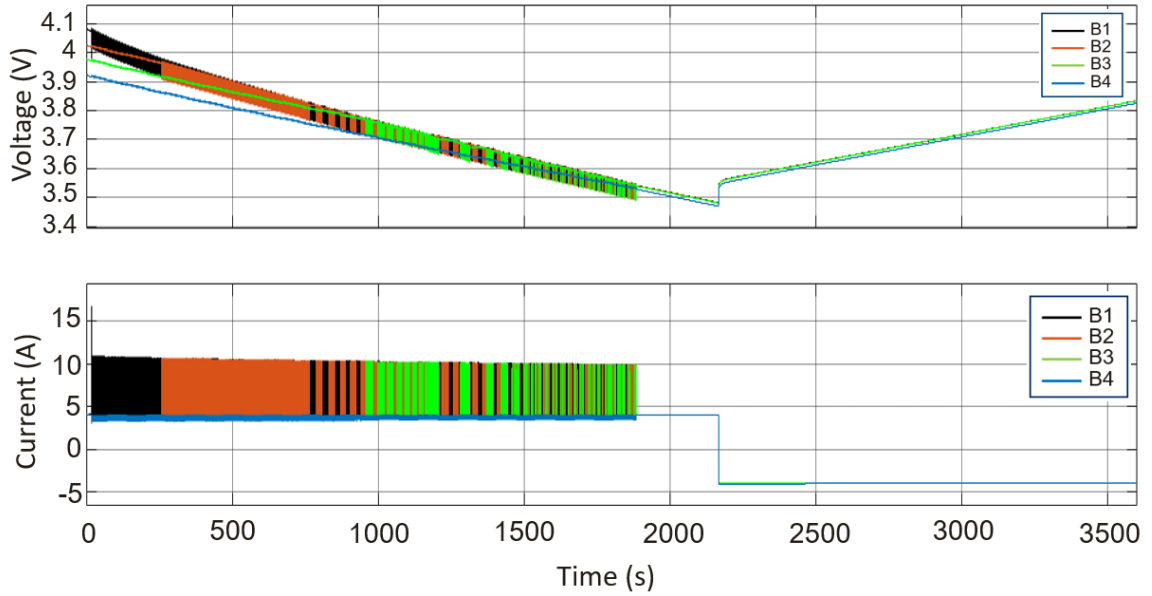


Figure 37 Discharge voltage and current

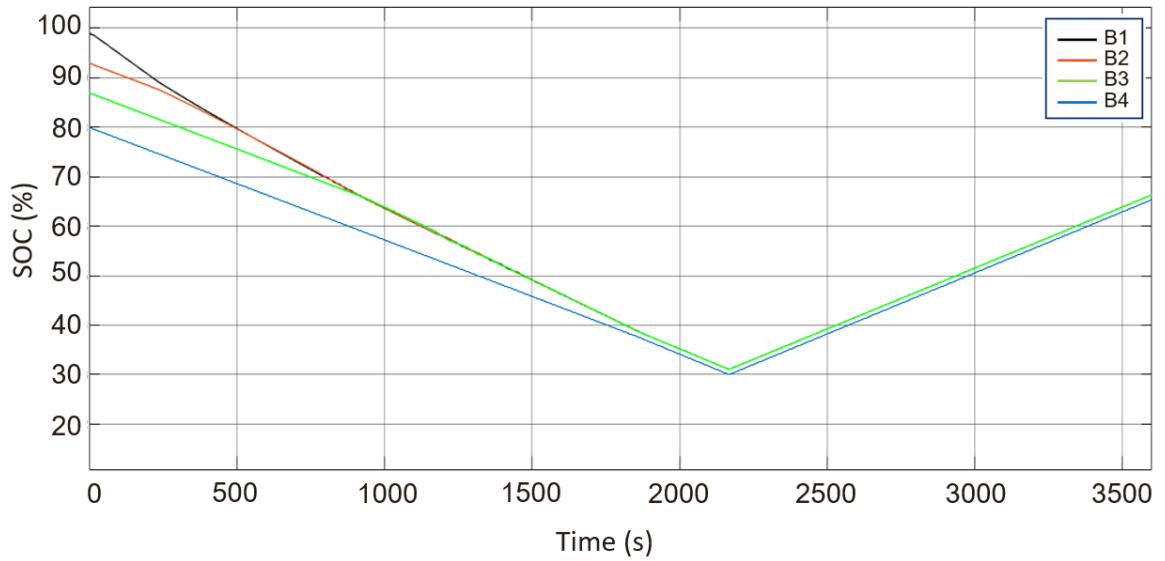


Figure 38 Discharge SOC

The SOC discharge of the cells shows smooth transition of the cells during balancing without any sharp charges and does not overshoot the balancing requirements. At the end of discharge balancing the cell maintain the 1% SOC difference since the only active system is the active balancer.

4.7 Comparison

Table 7 Balancer simulation comparison

Topology	State required	Balancing speed (seconds)	Component requirement (\$)	Efficiency	Temperature rise (°C)
Passive	4	21800	10.84	0	7.7
SC active	16	1060	64.55	N/A	12.2
Hybrid P/A	8	2250	29.7	83%	7.8

As mentioned in the literature review, the computational requirement of the passive balancer can be kept within a single state and utilize four sub states. As such the computational time is very fast and could keep up with near real time adjustments. On the other hand, the SC with C2P2C had the most internal states to keep track as well as the highest amount of control dedicated to the MOSFETs, this means that for every two states per cycle, the active balancer would need four states. The hybrid balancer can utilize both systems, thereby reducing the requirement from the active control, utilizing the state from the passive balancer, and only needing two substates which reduces the computation time.

The balancing speed is as expected with passive taking 21800 seconds to balance during charge, which is far too long for any reasonable attempt, but this is outside the passive balancer typical adjustment range. The active balancer has the fastest balancing speed at 1060 seconds but does experience some overbalancing of cells. The hybrid balancer does take longer than the active balancer in 1850 seconds and an additional 400 seconds due to the passive balancer but balances the cells more smoothly.

For component requirements the passive balancer has the least amount of requirement per cell, at one MOSFET, resistor and diode per cell. The hybrid topology utilizes the highest component count per cell since topology is a combination of the active and passive system. The Active topology uses two MOSFET per cell but does have a large amount of extra control MOSFETs for the shared DC/DC converter and must utilize a super capacitor.

For efficiency, the passive balancer is the worst since all excess energy is dissipated as heat, and the time efficiency is also quite bad. The hybrid balancer has a relatively good efficiency of 83% across the DC/DC converter, but the switching from the battery power flow control makes the system more inefficient from the ripples.

4.8 Summary

The design and simulation of a C2P flyback-based hybrid balancer is presented in this chapter along with efficiency and temperature behavior during charge and discharge balancing. The balancer simulation performs relatively quick balancing on a string of cells with a large voltage variation of 20% in 1870 seconds and allows for general cell cooling preventing the cells from experiencing high thermal degradation during charge. The cell with the highest SOC is the most actively used, but the system demonstrates that due to the balancing control, it experiences the least heat generation. Since the system also utilizes a passive balancer, it easily handles the full range of 20% to 1% variation easily reducing the time needed to charge in CV by preventing cell catchup in that mode. Notably for the active and hybrid balancer, to achieve the quick balancing speeds compared to literature, a high ripple is generated which may cause some battery ageing.

Chapter 5. Conclusions

This thesis primarily focused on developing a robust, high-fidelity lithium-ion battery model for SOH estimation and developing a hybrid cell balancing topology. Extensive experimental study is conducted which includes cycling of 21700 NMC lithium-ion battery at wide range of operating temperature and discharging condition to obtain the battery parameters for battery modelling. It has been demonstrated that the developed battery models are highly robust and accurate in SOH estimation and adaptive to the dynamics of ambient temperature and operating conditions. The proposed hybrid cell balancing strategy combined resistive passive balancing and DC-DC converter-based active balancing execute cell-to-pack balancing. The proposed hybrid cell balancing strategy not only enhanced the effective useful capacity and balancing speed but also reduced the maximum temperature rise of each cell which is beneficial for enhanced battery life due to lower degradation. It is noticed that with a 10% SOC difference, the balancing time required by the proposed topology is around 1850 seconds with a maximum cell temperature rise of 7.8°C and calculated efficiency of cell balancing is more than 83%. The topology reaps the benefit of both active and passive balancing of low cost and faster balancing with added lower temperature rise.

Chapter 1 provides an overview of the impact of temperature on battery degradation, existing battery models, the limitations of the existing battery models in considering the dynamics operating condition and impact of battery aging. The state-of-the-art techniques to enhance the battery life extensions and impact of lithium batteries on the economy and environment.

Chapter 2 provides a foundational knowledge and critical analysis of state-of-the-art cell battery balancing strategies, cell balancing control logics, current BMS architecture, and battery SOH estimation. The second chapter also discussed the applications of better battery models and more accurate state estimation in health-conscious battery management ensuring extended battery life and safer operation.

Chapter 3 lays the foundation of simulation systems by proposing two different battery models for highly precious SOH estimation adaptive to changes in ambient temperature and dynamic operating conditions. The single frequency low EIS based model was able to

estimate the capacity fade with statistical $R^2 = 0.90$ over 438 cycles utilizing only a 1 Hz frequency at 30% SOC. The SOH to thermal model was able to track the SOH over 80% of the cell's life based purely on the temperature rise of the cell ranging from 0.014 °C/s to 0.025°C/s from 100% SOH to 20% SOH respectively. These models can then be utilized within a BMS for low computation cost.

Chapter 4 presents the hybrid battery equalizing development, modeling, control methodology and efficiency calculations for determining usability of the topology. The equalizer was configured around balancing speed of 20% SOC difference in 1850 seconds with a nominal power transfer efficiency of 83% and maintaining the temperature of the cell under 26°C during charge and under 28°C during discharge. The topology is comparably faster than the industry standard of passive balancer, integrated to existing BMS equalizers, and economical compared to available transformer based BMS balancers and easy to replicate.

5.1 Future Work

- A greater in-depth integration of the predictive state of health battery models could be implemented to assist with balancing and state estimation. The model would preferably be reduced to data-tables for faster computation in a BMS. The thermal and degradation model could be used as a greater input to the control system, throttling the balancing speed and selected cell based on current temperature rise and estimated degradation rate.
- The thermal estimation can be implemented with cold temperature estimation, expanding the gradient table estimation of SOH. At the same time the model can also be implemented with early detection of a battery fire to meet the 5-minute warning of thermal runaway.
- The balancing method could be converted to a bidirectional converter allowing for the function of C2P and P2C balancing along with the passive balancer. This could potentially allow the balancers to have more distinct zones of operation depending on the needs of the individual cell. If bypass lines are also introduced, C2C could

also be an option within the topology allowing for an AC2C, P2C, and C2P battery balancer.

- Scaling or testing the balancing/BMS system to a greater number of cells or even small packs. This would assess the efficiency of the system for scalability. This can also be paired with a module level balancer to see dual stage balancing. The future implementation of this balancer can also be simulated with dynamic drive cycle and test balancing during regenerative braking.
- With the development of the SOH model and cell balancer, the combination can lead to further implementation of a multi-objective cell balancer which would consider all aspects and future effects of the equalizer. This could also be integrated with more inbuilt cell safety features such as balancing shut off or ignore a cell if the cell has a fault.

REFERENCES

- [1] M. Carrier, “Worldwide number of battery electric vehicles in use from 2016 to 2022,” *Statistica*, 2023. <https://www.statista.com/statistics/270603/worldwide-number-of-hybrid-and-electric-vehicles-since-2009/>
- [2] F. Lambert, “Tear down of 85 kWh Tesla battery pack shows it could actually only be a 81 kWh pack [Updated] | Electrek,” *Electrek*, 2016.
- [3] P. Cassani, “Modeling, design, and implementation of a novel battery cell equalizer for electric, hybrid electric, and plug-in hybrid electric vehicles.,” 2011.
- [4] Q. Wei, Y. Wu, S. Li, R. Chen, J. Ding, and C. Zhang, “Spent lithium ion battery (LIB) recycle from electric vehicles: A mini-review,” *Science of the Total Environment*. 2023. doi: 10.1016/j.scitotenv.2022.161380.
- [5] N. Chawla and M. Safa, “Sodium batteries: A review on sodium-sulfur and sodium-air batteries,” *Electronics (Switzerland)*. 2019. doi: 10.3390/electronics8101201.
- [6] W. Zhang, J. Yin, W. Wang, Z. Bayhan, and H. N. Alshareef, “Status of rechargeable potassium batteries,” *Nano Energy*. 2021. doi: 10.1016/j.nanoen.2021.105792.
- [7] F. Duarte Castro, L. Cutaia, and M. Vaccari, “End-of-life automotive lithium-ion batteries (LIBs) in Brazil: Prediction of flows and revenues by 2030,” *Resour. Conserv. Recycl.*, vol. 169, no. October 2020, p. 105522, 2021, doi: 10.1016/j.resconrec.2021.105522.
- [8] K. M. Winslow, S. J. Laux, and T. G. Townsend, “A review on the growing concern and potential management strategies of waste lithium-ion batteries,” *Resour. Conserv. Recycl.*, vol. 129, no. October 2017, pp. 263–277, 2018, doi: 10.1016/j.resconrec.2017.11.001.
- [9] S. Editors, C. Herrmann, and S. Kara, [*Sustainable Production, Life Cycle Engineering and Management*] Arno Kwade, Jan Diekmann (eds.) - *Recycling of Lithium-Ion Batteries_ The LithoRec Way (2018, Springer International*

- Publishing*).pdf. 2018. [Online]. Available: <http://link.springer.com/10.1007/978-3-319-70572-9>
- [10] Y. Qiao, S. Wang, F. Gao, X. Li, M. Fan, and R. Yang, “Toxicity analysis of second use lithium-ion battery separator and electrolyte,” *Polym. Test.*, vol. 81, no. August 2019, pp. 0–8, 2020, doi: 10.1016/j.polymertesting.2019.106175.
- [11] Y. Peng *et al.*, “A comprehensive investigation on the thermal and toxic hazards of large format lithium-ion batteries with LiFePO₄ cathode,” *J. Hazard. Mater.*, vol. 381, no. April 2019, 2020, doi: 10.1016/j.jhazmat.2019.120916.
- [12] L. C. Casals, B. Amante García, and C. Canal, “Second life batteries lifespan: Rest of useful life and environmental analysis,” *J. Environ. Manage.*, vol. 232, no. October 2017, pp. 354–363, 2019, doi: 10.1016/j.jenvman.2018.11.046.
- [13] M. Rasheed, M. Kamel, H. Wang, R. Zane, and K. Smith, “Investigation of Active Life Balancing to Recondition Li-ion Battery Packs for 2ndLife,” *2020 IEEE 21st Work. Control Model. Power Electron. COMPEL 2020*, 2020, doi: 10.1109/COMPEL49091.2020.9265808.
- [14] X. Li, T. Wang, L. Pei, C. Zhu, and B. Xu, “A comparative study of sorting methods for Lithium-ion batteries,” *IEEE Transp. Electrifi. Conf. Expo, ITEC Asia-Pacific 2014 - Conf. Proc.*, pp. 1–6, 2014, doi: 10.1109/ITEC-AP.2014.6940724.
- [15] Z. Xu *et al.*, “A novel clustering algorithm for grouping and cascade utilization of retired Li-ion batteries,” *J. Energy Storage*, vol. 29, no. 2, 2020, doi: 10.1016/j.est.2020.101303.
- [16] N. Yan, H. Zhao, X. Pan, G. Ma, and S. Ma, “Study on the Cluster Selection Method of Echelon Utilization Power Battery Based on Confidence Interval Estimation,” *IEEE Trans. Appl. Supercond.*, vol. 31, no. 8, pp. 10–13, 2021, doi: 10.1109/TASC.2021.3107831.
- [17] F. Zhang, M. M. U. Rehman, R. Zane, and D. Maksimović, “Hybrid balancing in a modular battery management system for electric-drive vehicles,” in *2017 IEEE Energy Conversion Congress and Exposition, ECCE 2017*, 2017. doi:

10.1109/ECCE.2017.8095835.

- [18] M. Uno, K. Yoshino, and K. Hasegawa, "Direct Cell-to-Cell Voltage Equalizer Using Capacitively-Isolated Parallel-Resonant Converter for Series-Connected Energy Storage Cells," in *Proceedings - 2018 IEEE 18th International Conference on Power Electronics and Motion Control, PEMC 2018*, 2018. doi: 10.1109/EPEPEMC.2018.8521841.
- [19] H. S, "Overview of cell balancing methods for Li-ion battery technology," *Energy Storage*, vol. 3, no. 2, Apr. 2021, doi: 10.1002/est2.203.
- [20] J. Gallardo-Lozano, E. Romero-Cadaval, M. I. Milanes-Montero, and M. A. Guerrero-Martinez, "Battery equalization active methods," *Journal of Power Sources*. 2014. doi: 10.1016/j.jpowsour.2013.08.026.
- [21] N. Ghaeminezhad, Q. Ouyang, X. Hu, G. Xu, and Z. Wang, "Active Cell Equalization Topologies Analysis for Battery Packs: A Systematic Review," *IEEE Trans. Power Electron.*, 2021, doi: 10.1109/TPEL.2021.3052163.
- [22] M. Uno and A. Kukita, "Double-switch equalizer using parallel-or series-parallel-resonant inverter and voltage multiplier for series-connected supercapacitors," *IEEE Trans. Power Electron.*, 2014, doi: 10.1109/TPEL.2013.2257867.
- [23] A. C. Baughman and M. Ferdowsi, "Double-tiered switched-capacitor battery charge equalization technique," *IEEE Trans. Ind. Electron.*, 2008, doi: 10.1109/TIE.2008.918401.
- [24] R. K. Vardhan, T. Selvathai, R. Reginald, P. Sivakumar, and S. Sundaresh, "Modeling of single inductor based battery balancing circuit for hybrid electric vehicles," in *Proceedings IECON 2017 - 43rd Annual Conference of the IEEE Industrial Electronics Society*, 2017. doi: 10.1109/IECON.2017.8216386.
- [25] A. F. Moghaddam and A. Van Den Bossche, "An Active Cell Equalization Technique for Lithium Ion Batteries Based on Inductor Balancing," in *Proceedings of 2018 9th International Conference on Mechanical and Aerospace Engineering, ICMAE 2018*, 2018. doi: 10.1109/ICMAE.2018.8467685.

- [26] N. Ganesh, G. Yadav, and C. K. Gowrishankara, "Analysis and implementation of inductor based active battery cell balancing topology," in *9th IEEE International Conference on Power Electronics, Drives and Energy Systems, PEDES 2020*, 2020. doi: 10.1109/PEDES49360.2020.9379358.
- [27] X. Cui, W. Shen, Y. Zhang, and C. Hu, "A fast multi-switched inductor balancing system based on a fuzzy logic controller for lithium-ion battery packs in electric vehicles," *Energies*, 2017, doi: 10.3390/en10071034.
- [28] Y. Shang, B. Xia, C. Zhang, N. Cui, J. Yang, and C. C. Mi, "An Automatic Equalizer Based on Forward-Flyback Converter for Series-Connected Battery Strings," *IEEE Trans. Ind. Electron.*, 2017, doi: 10.1109/TIE.2017.2674617.
- [29] Y. Li, J. Xu, X. Mei, and J. Wang, "A unitized multiwinding transformer-based equalization method for series-connected battery strings," *IEEE Trans. Power Electron.*, 2019, doi: 10.1109/TPEL.2019.2910205.
- [30] L. Liu *et al.*, "A Low-Cost Multiwinding Transformer Balancing Topology for Retired Series-Connected Battery String," *IEEE Trans. Power Electron.*, 2021, doi: 10.1109/TPEL.2020.3031904.
- [31] T. Alexandre Carvalho Maia, M. Berrehil El Kattel, T. Perpetuo Corrêa, A. V. Rocha, and B. J. C. Filho, "Battery energy management proposition for energy storage using active dc–dc converter," *Int. J. Circuit Theory Appl.*, 2022, doi: 10.1002/cta.3397.
- [32] A. F. Moghaddam and A. Van den Bossche, "A cuk converter cell balancing technique by using coupled inductors for lithium-based batteries," *Energies*, 2019, doi: 10.3390/en12152881.
- [33] T. Gottwald, Z. Ye, and T. Stuart, "Equalization of EV and HEV batteries with a ramp converter," *IEEE Trans. Aerosp. Electron. Syst.*, 1997, doi: 10.1109/7.570791.
- [34] S. K. Kollimalla and M. K. Mishra, "Analysis and control of buck-boost converter using average power balance control (APBC)," in *2012 Annual IEEE India*

Conference, INDICON 2012, 2012. doi: 10.1109/INDCON.2012.6420607.

- [35] A. Alvarez-Diazcomas, A. A. Estévez-Bén, J. Rodríguez-Reséndiz, M. A. Martínez-Prado, R. V. Carrillo-Serrano, and S. Thenozhi, “A review of battery equalizer circuits for electric vehicle applications,” *Energies*, vol. 13, no. 21, pp. 1–29, 2020, doi: 10.3390/en13215688.
- [36] C. Pascual and P. T. Krein, “Switched capacitor system for automatic series battery equalization,” in *Conference Proceedings - IEEE Applied Power Electronics Conference and Exposition - APEC*, 1997. doi: 10.1109/apec.1997.575744.
- [37] M. Y. Kim, C. H. Kim, J. H. Kim, and G. W. Moon, “A chain structure of switched capacitor for improved cell balancing speed of lithium-ion batteries,” *IEEE Trans. Ind. Electron.*, 2014, doi: 10.1109/TIE.2013.2288195.
- [38] V. L. Pham, V. T. Duong, and W. Choi, “A low cost and fast cell-to-cell balancing circuit for lithium-ion battery strings,” *Electron.*, vol. 9, no. 2, 2020, doi: 10.3390/electronics9020248.
- [39] D. Peng, M. Yan, C. Yang, Z. Fan, and C. Hong, “Equalization of series connected Lithium-ion battery based on state of charge in Electric Vehicle,” in *Proceedings of the World Congress on Intelligent Control and Automation (WCICA)*, IEEE, 2019, pp. 310–315. doi: 10.1109/WCICA.2018.8630431.
- [40] J. Han, S. Yang, X. Liu, and W. Yang, “An active direct cell-to-cell balancing circuit in continuous current mode for series connected batteries,” *Energies*, vol. 12, no. 20, 2019, doi: 10.3390/en12203978.
- [41] A. Samanta and S. Chowdhuri, “Active Cell Balancing of Lithium-ion Battery Pack Using Dual DC-DC Converter and Auxiliary Lead-acid Battery,” *J. Energy Storage*, 2021, doi: 10.1016/j.est.2020.102109.
- [42] A. M. Imtiaz and F. H. Khan, “‘Time shared flyback converter’ based regenerative cell balancing technique for series connected li-ion battery strings,” *IEEE Trans. Power Electron.*, 2013, doi: 10.1109/TPEL.2013.2257861.

- [43] Y. Liu, Y. Liu, C. Xia, M. Gu, W. Xin, and X. Men, "A novel active equalizer for Li-ion battery pack in electric vehicles," *Energy Procedia*, vol. 158, pp. 2649–2654, 2019, doi: 10.1016/j.egypro.2019.02.017.
- [44] A. Xu, S. Xie, and X. Liu, "Dynamic voltage equalization for series-connected ultracapacitors in EV/HEV applications," *IEEE Trans. Veh. Technol.*, 2009, doi: 10.1109/TVT.2009.2028148.
- [45] M. Y. Kim, C. H. Kim, S. Y. Cho, and G. W. Moon, "A cell selective charge equalizer using multi-output converter with auxiliary transformer," in *8th International Conference on Power Electronics - ECCE Asia: "Green World with Power Electronics"*, ICPE 2011-ECCE Asia, 2011. doi: 10.1109/ICPE.2011.5944610.
- [46] A. Farzan Moghaddam and A. Van Den Bossche, "Flyback Converter Balancing Technique for Lithium Based Batteries," *2019 8th Int. Conf. Mod. Circuits Syst. Technol. MOCAS 2019*, pp. 1–4, 2019, doi: 10.1109/MOCAS.2019.8741893.
- [47] L. A. Perișoară *et al.*, "Active Balancing for Efficient Management of a 4S1P LiFePO₄ Battery Pack," pp. 5–10, 2019.
- [48] Y. Shang, Q. Zhang, N. Cui, B. Duan, Z. Zhou, and C. Zhang, "Multicell-To-Multicell Equalizers Based on Matrix and Half-Bridge LC Converters for Series-Connected Battery Strings," *IEEE J. Emerg. Sel. Top. Power Electron.*, vol. 8, no. 2, pp. 1755–1766, 2020, doi: 10.1109/JESTPE.2019.2893167.
- [49] A. Samanta and S. Chowdhuri, "Active Cell Balancing of Lithium-ion Battery Pack Using Dual DC-DC Converter and Auxiliary Lead-acid Battery," *J. Energy Storage*, vol. 33, no. September, p. 102109, 2021, doi: 10.1016/j.est.2020.102109.
- [50] K. Friansa, I. N. Haq, E. Leksono, N. Tapran, D. Kurniadi, and B. Yulianto, "Battery module performance improvement using active cell balancing system based on Switched-Capacitor Boost Converter (S-CBC)," in *Proceeding - 4th International Conference on Electric Vehicular Technology, ICEVT 2017*, 2018. doi: 10.1109/ICEVT.2017.8323541.

- [51] A. Sani, C. K. Hu, Y. C. Hsieh, H. J. Chiu, and J. Y. Lin, "Switched-capacitor charge equalization circuit for series-connected batteries," in *2016 IEEE 2nd Annual Southern Power Electronics Conference, SPEC 2016*, 2016. doi: 10.1109/SPEC.2016.7846016.
- [52] F. Baronti, G. Fantechi, R. Roncella, and R. Saletti, "High-efficiency digitally controlled charge equalizer for series-connected cells based on switching converter and super-capacitor," *IEEE Trans. Ind. Informatics*, 2013, doi: 10.1109/TII.2012.2223479.
- [53] B. Jiang, Y. Liu, X. Huang, and R. R. R. Prakash, "A New Battery Active Balancing Method with Supercapacitor Considering Regeneration Process," in *IECON Proceedings (Industrial Electronics Conference)*, 2020. doi: 10.1109/IECON43393.2020.9254839.
- [54] X. Lu and F. Anariba, "Fostering innovation through an active learning activity inspired by the baghdad battery," *J. Chem. Educ.*, 2014, doi: 10.1021/ed400869c.
- [55] C. F. J. Francis, I. L. Kyratzis, and A. S. Best, "Lithium-Ion Battery Separators for Ionic-Liquid Electrolytes: A Review," *Advanced Materials*. 2020. doi: 10.1002/adma.201904205.
- [56] X. R. Chen, Y. X. Yao, C. Yan, R. Zhang, X. B. Cheng, and Q. Zhang, "A Diffusion--Reaction Competition Mechanism to Tailor Lithium Deposition for Lithium-Metal Batteries," *Angew. Chemie - Int. Ed.*, 2020, doi: 10.1002/anie.202000375.
- [57] H. Zhang, G. G. Eshetu, X. Judez, C. Li, L. M. Rodriguez-Martínez, and M. Armand, "Electrolyte Additives for Lithium Metal Anodes and Rechargeable Lithium Metal Batteries: Progress and Perspectives," *Angewandte Chemie - International Edition*. 2018. doi: 10.1002/anie.201712702.
- [58] M. Wood *et al.*, "Chemical stability and long-term cell performance of low-cobalt, Ni-Rich cathodes prepared by aqueous processing for high-energy Li-Ion batteries," *Energy Storage Mater.*, vol. 24, pp. 188–197, Jan. 2020, doi:

10.1016/J.ENSM.2019.08.020.

- [59] C. Julien, A. Mauger, A. Vjih, and K. Zaghib, *Lithium Batteries: Science and Technology*. 2015. doi: 10.1007/978-3-319-19108-9.
- [60] N. Omar *et al.*, “Lithium iron phosphate based battery - Assessment of the aging parameters and development of cycle life model,” *Appl. Energy*, vol. 113, pp. 1575–1585, 2014, doi: 10.1016/j.apenergy.2013.09.003.
- [61] A. L. Michan, G. Divitini, A. J. Pell, M. Leskes, C. Ducati, and C. P. Grey, “Solid Electrolyte Interphase Growth and Capacity Loss in Silicon Electrodes,” *J. Am. Chem. Soc.*, vol. 138, no. 25, pp. 7918–7931, 2016, doi: 10.1021/jacs.6b02882.
- [62] V. A. Marcis, A. V. J. S. Praneeth, L. Patnaik, and S. S. Williamson, “Analysis of CT-CV Charging Technique for Lithium-ion and NCM 18650 Cells,” *2020 IEEE Int. Conf. Power Electron. Smart Grid Renew. Energy, PESGRE 2020*, no. 1, pp. 947–952, 2020, doi: 10.1109/PESGRE45664.2020.9070505.
- [63] A. Rastegarpanah, J. Hathaway, and R. Stolkin, “Rapid model-free state of health estimation for end-of-first-life electric vehicle batteries using impedance spectroscopy,” *Energies*, vol. 14, no. 9, 2021, doi: 10.3390/en14092597.
- [64] S. Surya, V. Marcis, and S. Williamson, “Core Temperature Estimation for a Lithium ion 18650 Cell,” *Energies*, vol. 14, no. 1, p. 87, 2020, doi: 10.3390/en14010087.
- [65] M. Swierczynski, D. Stroe, S. K. Kær, and A. Øst, “Calendar Ageing of LiFePO₄ / C Batteries in the Second Life Applications Keywords,” pp. 2–9.
- [66] L. L. Li, Y. H. Ren, C. H. Wang, and C. T. Jen, “A new method to estimate the state of charge of the green battery,” *Microelectron. Reliab.*, vol. 79, pp. 306–313, 2017, doi: 10.1016/j.microrel.2017.07.031.
- [67] P. Shrivastava, T. Kok Soon, M. Y. I. Bin Idris, S. Mekhilef, and S. B. R. S. Adnan, “Combined State of Charge and State of Energy Estimation of Lithium-Ion Battery Using Dual Forgetting Factor-Based Adaptive Extended Kalman Filter for Electric Vehicle Applications,” *IEEE Trans. Veh. Technol.*, vol. 70, no. 2, pp.

1200–1215, 2021, doi: 10.1109/TVT.2021.3051655.

- [68] H. Pang, L. Guo, L. Wu, and X. Jin, “An enhanced temperature-dependent model and state-of-charge estimation for a Li-Ion battery using extended Kalman filter,” *Int. J. Energy Res.*, vol. 44, no. 9, pp. 7254–7267, 2020, doi: 10.1002/er.5435.
- [69] Z. Xia and J. A. Abu Qahouq, “State-of-Charge Balancing of Lithium-Ion Batteries with State-of-Health Awareness Capability,” *IEEE Trans. Ind. Appl.*, 2021, doi: 10.1109/TIA.2020.3029755.
- [70] A. Carnovale and X. Li, “A modeling and experimental study of capacity fade for lithium-ion batteries,” *Energy and AI*, vol. 2, p. 100032, 2020. doi: 10.1016/j.egyai.2020.100032.
- [71] E. Martinez-Laserna *et al.*, “Technical Viability of Battery Second Life: A Study from the Ageing Perspective,” *IEEE Trans. Ind. Appl.*, vol. 54, no. 3, pp. 2703–2713, 2018, doi: 10.1109/TIA.2018.2801262.
- [72] B. Jiang, J. Zhu, X. Wang, X. Wei, W. Shang, and H. Dai, “A comparative study of different features extracted from electrochemical impedance spectroscopy in state of health estimation for lithium-ion batteries,” *Appl. Energy*, vol. 322, no. 2012, p. 119502, 2022, doi: 10.1016/j.apenergy.2022.119502.
- [73] Q. Zhang, C. G. Huang, H. Li, G. Feng, and W. Peng, “Electrochemical Impedance Spectroscopy based State of Health Estimation for Lithium-ion Battery Considering Temperature and State of Charge Effect,” *IEEE Trans. Transp. Electr.*, vol. 7782, no. ML, 2022, doi: 10.1109/TTE.2022.3160021.
- [74] H. Tian, P. Qin, K. Li, and Z. Zhao, “A review of the state of health for lithium-ion batteries: Research status and suggestions,” *Journal of Cleaner Production*. 2020. doi: 10.1016/j.jclepro.2020.120813.
- [75] K. Mc Carthy, H. Gullapalli, K. M. Ryan, and T. Kennedy, “Electrochemical impedance correlation analysis for the estimation of Li-ion battery state of charge, state of health and internal temperature,” *J. Energy Storage*, vol. 50, no. March, p. 104608, 2022, doi: 10.1016/j.est.2022.104608.

- [76] C. Lyu, T. Zhang, W. Luo, G. Wei, B. Ma, and L. Wang, “Fast Time Domain Impedance Spectroscopy,” *2019 14th IEEE Conf. Ind. Electron. Appl.*, pp. 2142–2147, 2019.
- [77] M. Galeotti, L. Cinà, C. Giammanco, S. Cordiner, and A. Di Carlo, “Performance analysis and SOH (state of health) evaluation of lithium polymer batteries through electrochemical impedance spectroscopy,” *Energy*, vol. 89, pp. 678–686, 2015, doi: 10.1016/j.energy.2015.05.148.
- [78] J. Huang, H. Ge, Z. Li, and J. Zhang, “Dynamic Electrochemical Impedance Spectroscopy of a Three-Electrode Lithium-Ion Battery during Pulse Charge and Discharge,” *Electrochim. Acta*, 2015, doi: 10.1016/j.electacta.2015.07.017.
- [79] P. A. Lindahl, M. A. Cornachione, and S. R. Shaw, “A time-domain least squares approach to electrochemical impedance spectroscopy,” *IEEE Trans. Instrum. Meas.*, 2012, doi: 10.1109/TIM.2012.2210457.
- [80] K. Mc Carthy, H. Gullapalli, K. M. Ryan, and T. Kennedy, “Review—Use of Impedance Spectroscopy for the Estimation of Li-ion Battery State of Charge, State of Health and Internal Temperature,” *J. Electrochem. Soc.*, 2021, doi: 10.1149/1945-7111/ac1a85.
- [81] M. Kwiecien, J. Badedda, M. Huck, K. Komut, D. Duman, and D. U. Sauer, “Determination of SoH of Lead-Acid Batteries by Electrochemical Impedance Spectroscopy,” pp. 1–23, doi: 10.3390/app8060873.
- [82] D. Xi, J. Wang, and X. Guo, “Review—Use of Impedance Spectroscopy for the Estimation of Li-ion Battery State of Charge, State of Health and Internal Temperature,” *Biosci. Rep.*, 2009.
- [83] T. T. Nguyen, V. L. Tran, and W. Choi, “Development of the intelligent charger with battery State-Of-Health estimation using online impedance spectroscopy,” in *IEEE International Symposium on Industrial Electronics*, 2014. doi: 10.1109/ISIE.2014.6864656.
- [84] Y. X. Lin, Z. Liu, K. Leung, L. Q. Chen, P. Lu, and Y. Qi, “Connecting the

irreversible capacity loss in Li-ion batteries with the electronic insulating properties of solid electrolyte interphase (SEI) components,” *J. Power Sources*, vol. 309, pp. 221–230, Mar. 2016, doi: 10.1016/j.jpowsour.2016.01.078.

- [85] Z. Guo, B. Y. Liaw, X. Qiu, L. Gao, and C. Zhang, “Optimal charging method for lithium ion batteries using a universal voltage protocol accommodating aging,” *J. Power Sources*, vol. 274, pp. 957–964, Jan. 2015, doi: 10.1016/j.jpowsour.2014.10.185.
- [86] A. Samanta, A. Huynh, M. Sharma, V. Marcis, and S. Williamson, “Supercapacitor and Bidirectional DC-DC Converter-based Active Charge Balancing Scheme for Lithium-ion Batteries,” in *2022 IEEE Energy Conversion Congress and Exposition, ECCE 2022*, 2022. doi: 10.1109/ECCE50734.2022.9947732.
- [87] W. C. Lee, D. Drury, and P. Mellor, “An integrated design of active balancing and redundancy at module level for electric vehicle batteries,” *2012 IEEE Transp. Electrification Conf. Expo, ITEC 2012*, 2012, doi: 10.1109/ITEC.2012.6243504.

Appendices

Appendix A.

Publications

Conference Publications

1. A. Huynh, A. Samanta, C. Chetri, L. Anekal, and S. Williamson, "A Smart, Health-conscious, Dual-stage Hybrid Lithium-ion Battery Cell Voltage Balancing Strategy." IEEE Energy Conversion Congress, and Exposition (ECCE), Nashville, Tennessee, 2023. [Accepted]
2. A. Huynh, A. Samanta, C. Chetri, S. Williamson, "Online determination of lithium-ion battery state of health based on normalized change of state of temperature for e-mobility applications." Accepted- IEEE Transportation Electrification Conference & Expo (ITEC), Detroit, Michigan, 2023.
3. A. Samanta, A. Huynh, N. Shrestha, S. Williamson, "Combined data-driven and online impedance measurement-based lithium-ion battery state of health estimation for electric vehicle battery management systems." IEEE Applied Power Electronics Conference and Exposition (APEC), Orlando, Florida, 2023.
4. C. Chetri, A. Huynh, and S. S. Williamson, "A Comprehensive Review of Active EV Battery Cell Voltage Balancing Systems: Current Issues and Prospective Solutions." 2022 IEEE 1st Industrial Electronics Society Annual On-Line Conference (ONCON), kharagpur, India, 2022, pp. 1-6, doi: 10.1109/ONCON56984.2022.10126563.
5. A. Samanta, A. Huynh, E. Rutovic and S. Williamson, "Rapid Thermal Modeling and Discharge Characterization for Accurate Lithium-ion Battery Core Temperature Estimation," IECON 2022 – 48th Annual Conference of the IEEE Industrial Electronics Society, Brussels, Belgium, 2022, pp. 1-6.
6. A. Samanta, A. Huynh, M. Sharma, V. Marcis and S. Williamson, "Supercapacitor and Bidirectional DC-DC Converter-based Active Charge Balancing Scheme for

Lithium-ion Batteries “, IEEE Energy Conversion Congress and Exposition (ECCE), Detroit, MI, USA, 2022, pp. 1-7.

Journals

8. A. Samanta, A. Huynh, M. Sharma, S. Williamson,” Supercapacitor and Kalman Filter Controlled Bidirectional DC-DC Converter for Active Charge Balancing of Lithium-ion Batteries”, IEEE-IAS Transportation Systems Committee. [Under Review]

7.3Prints

9. A. Samanta, A. Huynh, L. Anekal, C. Chetri, S. Williamson, “Power Electronic Converters and Systems.” 2nd Edition, 2023 [under review]

Appendix B.

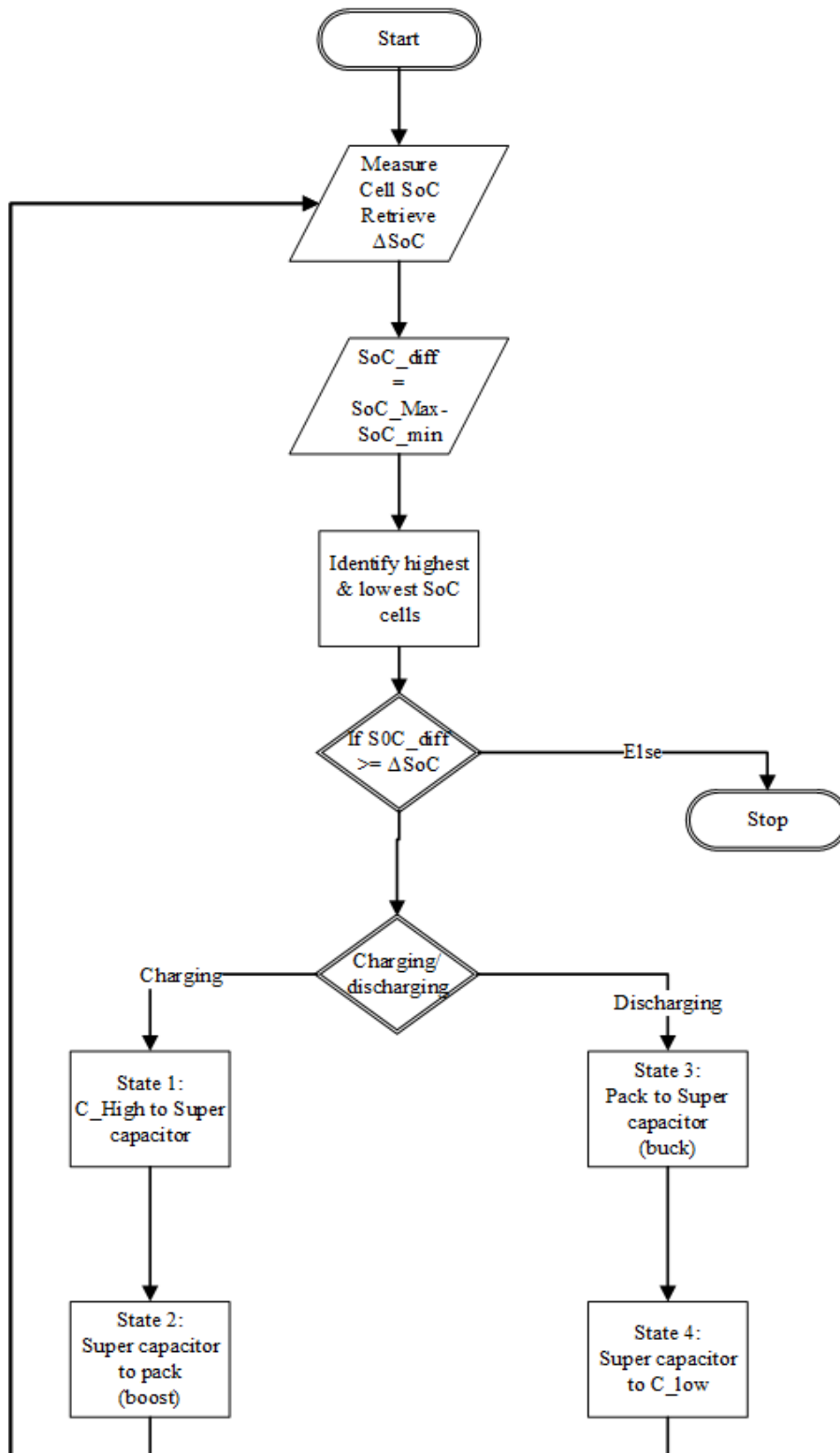


Figure 39 Super capacitor C2P2C balancer